

Analysis of the mechanism of spongiform degeneration
induced by neuropathogenic mouse hepatitis virus

2014

Hiromi Kashiwazaki

Table of Contents

Abstract·····p. 1

Introduction·····p. 2~4

Materials and Methods·····p. 5~9

Results·····p. 10~15

Discussion·····p. 16~19

References·····p. 20~24

Figures·····Figure. 1 ~ 16, p. 25~45

Table·····p. 46

Abstract

JHMV-cl-2 strain (cl-2) exhibits extremely high neurovirulence. In contrast, srr7 cloned as a soluble receptor-resistant mutant from the cl-2 virus also exerts neurovirulence like its maternal virus, but with a lower virulence than cl-2. An outstanding difference between cl-2 and srr7 is that the former spreads in both MHV receptor (MHVR)-dependent and -independent fashions, whereas srr7 lacks the ability to spread in an MHVR-independent fashion. We demonstrated the detailed neuropathologic feature of infection with srr7. During the course of infection with srr7, the distinct vacuolar degeneration could be detectable at 48 hours post-inoculation (pi) in the area where no viral antigens were detected. We also demonstrated that all kinds of cell population of immuno-competent cells, at every time point between 12 and 48 hours pi were infected with both cl-2 and srr7. The next viral spread was observed in the ependymal cells and nestin-positive immature cells at 48 hours pi when spongiosis became apparent. The manner of viral spread after infection and area of lesions with cl-2 or srr7 encouraged us to investigate the possibility that neuropathogenesis might be induced by the indirect effects of infection including cytokines. The levels of several cytokines were also increased in the pons during this time after infection with both cl-2 and srr7. Surprisingly, high levels of circulating cytokines were detected in the brain of mice infected with cl-2 compared with that of mice infected with srr7. Furthermore, the constructions of the fibers which mimic the fibroblastic reticular network, which composes a conduit system and functions as immune communication network in lymphoid organs were observed in the brain. These observations indicate that immune communication in the brain parenchyma might contribute to the different neuropathogenesis or spongiotic degeneration observed in srr7-infection.

1. Introduction

Mouse hepatitis virus (MHV), a member of the coronavirus family, is an enveloped virus with single-stranded, positive-sense genomic RNA that is about 30 kilobases long. MHV causes different types of disease, such as hepatitis, enteritis, and encephalomyelitis. Interest in the pathogenicity of murine coronaviruses, in particular JHM strains of MHV (JHMV), has centred on their ability to produce both acute and chronic central nervous system (CNS) diseases. Several different molecules function as MHV receptors (Beauchemin et al. 1999; Chen et al. 1995; Nédellec et al. 1994), among which carcinoembryonic antigen-related cell adhesion molecule 1 (CEACAM1 or MHVR) is the most prevalent (Ohtsuka et al. 1996; Rao et al. 1997). Infection in most tissues is thought to be mediated by MHVR, since the distribution of viral protein in the tissue is closely related to the MHVR distribution (Godfraind et al. 1995). MHVR is abundantly expressed in epithelia, vessel endothelia, granulocytes, monocytes, macrophages, T cells, B cells, NK cells, and platelets (Greicius et al. 2003; Kammerer et al. 2001; Moller et al. 1996; Odin et al. 1988). The viral protein that interacts with MHVR is the spike (S) protein. The S protein is synthesized as a 180- to 200-kDa protein that is cleaved into two subunits by host-derived protease (Sturman et al. 1985). The N-terminal subunit, called S1, forms the outermost knob-like structure of the spike, and the C-terminal S2 subunit forms the stem-like structure beneath the knob (de Groot et al. 1987; Taguchi et al. 2002).

There are many strains of mouse hepatitis virus (MHV), viruses that infect mainly the brain and liver. Based on previous studies, which used numerous variant viruses selected for resistance to neutralizing monoclonal antibodies, an association was made between various mutations or deletions in the S gene and neuroattenuation of the different strains of MHV (Gallagher et al. 1992). The use of recombinant MHV viruses with a modified spike (S) glycoprotein has definitively identified the S protein as a major determinant of neurovirulence. Among JHMVs, JHMV-cl-2 strain (cl-2) exhibits extremely high neurovirulence (Taguchi et al. 1985). In mixed neural cell cultures, cl-2 induced syncytia in most of the cells including neurons. Clinically, mice infected with cl-2 developed CNS signs, such as ataxic gait and hind-limb paralysis, from the second to third days pi. In contrast, srr7 cloned as a soluble receptor-resistant mutant from the cl-2 virus also exerts neurovirulence like its maternal virus, but with a lower virulence than cl-2. srr7, which infects and spreads solely in an MHVR-dependent fashion (Taguchi et al. 2002), infected a limited number of microglia marker-positive cells and infection did not spread, indicating that microglial cells are the initial target for MHV infection and that cl-2 spreads from initially infected microglia to a variety of cells in an MHVR-independent fashion, which suggested that MHVR is essential for the initiation of MHV infection in the brain. Although srr7 surface proteins show binding activity through the S1 region of the surface protein to the viral receptor, similar to that of wild-type cl-2 protein, srr7 is less virulent than cl-2. The reduced virulence and infectivity of srr7 compared with those of cl-2 could be attributed to the mutation of a single amino acid at position 1114 (Leu to Phe) in the S2 subunit of the viral surface protein (Saeki et al. 1997), which is not involved in receptor binding activity.

However, there is no difference in the viral growth rate during the initial phase of infection between these two strains as determined by a titration assay. In addition, the neuropathologic feature of infection with *srr7* has not been studied. It might be possible that only dependency on MHVR or ability to infect neurons do not contribute to the different neuropathogenesis induced by infection with *cl-2* and *srr7*.

Previously, we evaluated viral spread in the central nervous system in the early phase post-infection (Takatsuki et al. 2010). Initial viral antigens were detected in the infiltrating cells that appeared in the subarachnoidal space of mouse brains infected with viruses, without spreading into the brain parenchyma including the virus injection sites (Kashiwazaki et al. 2011a; Takatsuki et al. 2010). These two viruses exhibit similarities in the initial infection before 24 hours pi, when the viral antigens are not yet observable in the infected brain parenchyma, i.e., at 12 hours pi; both of the viruses were already found to have infected the monocyte lineage infiltrating into the subarachnoidal space, inducing viral- and F4/80-antigen positive syncytial giant cells. Besides these inflammatory cells, viral antigens during the early phase of infection were detected in the ependymal cells indicating that the ventricular wall was also the target site during the initial phase of infection with viruses. Furthermore, at the same time, viral antigens were detected in the splenic red pulp of mice infected with either virus, although the viruses are inoculated into the frontal lobe of the brain. However, among the other infiltrating cells in the subarachnoidal space or cells in the spleen and ventricular wall, many of the infected cells remained uncharacterized.

Besides these inflammatory cells, viral antigens during the early phase of infection were detected in the fibrous structures of the meninx. Later, at 24 hours pi, viral antigen-positive fibrous structures were observed deep in the brain parenchyma. These viral antigen-positive structures might be correlated with the CD31-positive blood vessel architecture or unrelated, and also be correlated with CD11b antigen or unrelated as well.

Previous investigation at 12 hours pi for mice either with *cl-2* or *srr7* infection revealed no apparent destruction of the brain parenchyma, which appeared after 24 hours pi with inflammatory cell infiltration. The neuropathological changes induced by *cl-2* or *srr7* infection after 48 hours pi were same, with exception of description about an appearance of infected syncytial giant cells, as already published reports, which demonstrated different distribution and intensity of *cl-2* and *srr7*-induced lesions, i.e. rapid and widespread destructive changes in the grey matter of the brain infected with *cl-2*, whereas *srr7* infection induced lesions after longer incubation period than *cl-2* did, with predilection to the white matter. An outstanding difference between *cl-2* and *srr7* is that the former spreads in both MHVR-dependent and -independent fashions, whereas *srr7* lacks the ability to spread in an MHVR-independent fashion. Therefore, the difference in this pathogenesis could be due to whether the virus spreads in an MHVR-independent fashion or not. However, the reasons why these strains show predilection sites for lesions remained unclear. The detailed neuropathologic feature of infection with *srr7* has not been studied.

The manner of viral spread after infection and area of lesions with *cl-2* or *srr7* mentioned above indicates that routes of viral spread into the brain parenchyma may contribute the different

neuropathogenesis. Our investigation to identify the viral entry route was focused on the area between the fourth ventricle and meninges in the cerebellopontine angle because the viral antigens are often found in this area during the early phase of infection. Also, at this site, there is a conduit, the foramen of Luschka, for cerebrospinal fluid to flow from the ventricle into the subarachnoid space. Another intriguing feature of viral antigen localization after infection with cl-2 or srr7 is that the viral antigens were found in fibrous structures, which appeared to be extracellular matrix (ECM), in the brain and spleen. Viruses proliferate and produce viral antigens in living cells, and it is unusual to find them in the ECM. Such colocalization of viral antigen or viral particles with ECM has been reported to occur in the lymphoid organs (Steele et al. 2009). This ECM colocalized with viral antigens observed by Steele et al. is the component of filamentous structures called fibroblastic reticular network (FRN). For example, after infection with LCMV, viral antigens are found colocalized with the components of reticular fibers, including collagen III and laminin, in the spleen (Mueller et al. 2007). Similar phenomena have been reported on infection with extremely virulent viruses, such as Ebola, Marburg, and Lassa viruses (Steele et al. 2009). These viruses infect fibroblastic reticular cells (FRCs) in the lymphoid organs, followed by immune dysfunction, allowing viral persistence (Mueller et al. 2007) or tissue destruction (Steele et al. 2009).

FRCs are considered to maintain reticular fibers, which comprise a fibroblastic reticular network (FRN) in the lymph nodes and spleen (Mueller et al. 2007). Erasmus University Rotterdam-thymic reticulum antibody 7 (ER-TR7) has been used to define FRCs (Van Viliet et al. 1986), although the antigen of ER-TR7 has yet to be determined. The reticular fiber that comprises the FRN is around 1 μm in diameter, and contains collagen fibers as a core surrounded by an ER-TR7 antigen-positive microfibrillar layer, and further enclosed with basement lamina at the outer surface. The entire fiber is largely ensheathed by FRCs. The FRN has been reported to function as a conduit system for immunocompetent cells and inflammation-associated molecules such as cytokines and ligands or foreign antigens to reach appropriate sites and cause an immune reaction in the lymph nodes and spleen (Nolte et al. 2003), or to guide the homing of cells (Bajénoff et al. 2008).

This type of structure is not restricted to lymphoid organs, and there is evidence that similar scaffolds guide migration of immune cells in other sites including brain (Egen et al. 2008; Mrass et al. 2006; Mrass and Weninger 2006; Wilson et al. 2009). This led us to hypothesize that FRN might be the specific route for transporting viral particles, infected cells or cytokines within the brain and contribute to pathogenesis induced by cl-2 and srr7.

2. Materials and methods

Animals and Viruses

Fucosyltransferase 9 knockout (Fut9^{-/-}) mice with the BALB/c background (Kudo et al. 2007) and specific-pathogen-free inbred BALB/c mice purchased from Charles River (Tokyo, Japan) were housed in a specific pathogen-free animal facility, and were kept according to the guidelines set by the committee of our university. Mock-infected mice were given an equivalent amount of Dullbecco's modified minimal essential medium (DMEM; GIBCO, Staley Road, Grand Island, NY, USA) to ensure whether the mechanical damage resulting from injection affect antigen expression. For infection, mice were transferred to the P3-level laboratory. Each mouse was injected with 1×10^2 of the srr7 or cl-2 virus into the right frontal lobe under deep anesthesia. Infected mice were killed at intervals, and organs were aseptically isolated from animals and stored at -80°C until titration. These organs in phosphate-buffered saline (PBS; Nissui, Tokyo, Japan) were homogenized with a glass homogenizer and centrifused at 5000 rpm for 5minutes. The infectivity in the supernatants was measured by a plaque assay using DBT cells, as described previously (Matsuyama et al. 2001). DBT cells were grown in DMEM supplemented with 5% fetal bovine serum (FBS; Sigma, Tokyo, Japan) and cultured at 37°C with humidity and 5% CO₂.

Cytospin Procedure

Single-cell suspensions were prepared by teasing the spleens in phosphate-buffered saline with DMEM supplemented with 1% FBS, and passing them through a stainless mesh. They were centrifuged and the resulting cell pellets were suspended in a 0.83% NH₄Cl-Tris buffer (pH 7.65) to lyse the red blood cells. The spleen cells were suspended in PBS (Nissui) containing 0.02 % Ethylenediaminetetraacetic acid tetrasodium salt dihydrate and 0.5% bovine serum albumin (both from Sigma, Tokyo, Japan) for the cytopsin procedure. A total of 0.1 ml of the fluid sample containing 1×10^6 cells was added to the chamber fixed and secured on the glass by a metal clip. Filter cards, sample chambers, and metal clips were all obtained from SHANDON, Pittsburgh, PA, USA. After spinning at 2000 rpm for 4 minutes, slides were removed from the cytopsin chamber, and were further fixed in 100% alcohol for 2 minutes and acetone for 5 minutes (Wako, Osaka, Japan), and then stored at -35°C until use.

Fluorescent Tracers.

Ten-kilodalton lysine fixable dextran, Texas Red was purchased from Invitrogen (USA). Tracers were injected intravenously in 200 µl of PBS (Nissui), and mice were perfused with PBS followed by 4% paraformaldehyde from the aorta via the left ventricle after 10 minutes. Spleens and brains were immersion-fixed overnight in 4% paraformaldehyde, followed by immersion in PBS for 1hour on a rotator (Iuchi Seiei-do Inc., Osaka, Japan). The tissues were then rinsed stepwisely in PBS or sterilized water supplemented with increasing concentrations of sucrose (Wako, Osaka, Japan), followed by a final rinse with 25% sucrose. All steps were performed at 4 °C in a rotator

(TAAB Laboratories, Reading, UK). Tissues were isolated and embedded in OCT compound (Sakura, Tokyo, Japan). Tissue blocks were frozen in dry ice. Ten-micrometer sections were cut using a cryostat (Sakura), air dried, and stored at -30°C until stained. In order to identify and localize internalized dextran, immunofluorescence staining was performed as described below, and slides were examined by fluorescence microscopy.

Primary Cell Cultures

Primary mixed neural cell culture were established from the forebrains of neonate mice as described previously (Nakagaki et al. 2005), with minor modifications. Briefly, newborn mice were decapitated, and their cerebral hemispheres were aseptically collected in PBS (Nissui). The hemispheres were minced and passed through a stainless mesh. The tissue pieces were dissociated by gently pipetting up. The resultant suspension was centrifuged at 1000 rpm for 7 minutes at 0°C, the supernatant was discarded, and the pellet was resuspended in DMEM (GIBCO) supplemented with 1% FBS, containing dispase (Roche, Branchburg, NJ) and collagenase (Invitrogen, Carlsbad, CA, USA). Prior to use, dispase and collagenase was heated at 37°C for 10 minutes. DNase was added to cell suspension before counting cells. After centrifugation, the cells were washed with DMEM supplemented with 1% FBS. Cells were plated at a density of 3×10^4 cells per well in eight-well plastic chamber slides (Nalge Nunc International, NY, USA) in DMEM supplemented 10% with heat-inactivated FBS (Sigma) containing B27 supplements (Invitrogen). Experiments were performed in 7- to 10-day-old cultures. Several fields were compared for intensity of positive immunostaining by using a BZ-analyzer (Keyence, Osaka, Japan). Background fluorescence for ER-TR7 was determined as the mean fluorescence intensity from an area containing cells that did not express the constructs, and it was subtracted from the overall intensity.

Antibodies.

All antibodies used for immunohistochemistry, immunofluorescent staining, the dilutions and conditions under which they were used are listed in Table 1.

Immunohistochemistry

After exsanguination of the infected animals under deep anesthesia, removed parts of the brain were fixed in 4% paraformaldehyde buffered with 0.12 M phosphate to obtain paraffin-embedded sections for histological staining with hematoxylin-eosin (HE) or HE and luxol fast blue, and for enzyme immunohistochemistry (Watanabe and Takase-Yoden 2006). Viral antigens were visualized using the rabbit polyclonal antibody, SP-1, or mouse monoclonal antibody (MAb) (Matsuyama et al. 2001; Nakagaki et al. 2005). Rat anti-mouse F4/80 either unlabeled or biotin-conjugated, rat anti-mouse CD11b biotin-conjugated, rabbit or mouse anti-GFAP were used for cell identification. As a second or third application, biotinylated donkey anti-rabbit IgG (Amersham, Tokyo, Japan), goat anti-mouse IgG (Cappel, Solon, OH, USA), biotin-conjugated

donkey anti-mouse IgG (Rockland, Gilbertsville, PA, USA), rabbit peroxidase anti-peroxidase complexes (Cappel, Downington, PA, USA), or avidin-peroxidase conjugate (Molecular Probe, Eugene, OR, USA) was used, as described previously. After deparaffinization, sections were incubated with 50% normal horse or 50% normal mixed serum (fetal calf, calf, pig, and horse) diluted in PBS prior to the first antibody application to block non-specific antibody binding. The non-specific activity of endogenous peroxidase was blocked after primary antibody incubation by incubating sections with 0.3% H₂O₂ in methanol. Washes in PBS were carried out between each step. For the peroxidase reaction, 0.2 mg/mL 3,3'-diaminobenzidine tetrahydrochloride (DAB) (Wako, Osaka, Japan) in 0.1 M Tris buffer (pH 7.6) was used to obtain brown staining. For double staining, horseradish peroxidase localization was revealed using 4-chloro-1-naphthol (Wako) substrate, resulting in purple staining.

Double and triple immunofluorescence

Ten-µm serial sections of tissue were cut using a Tissue-Tek II Cryostat (Sakura, Tokyo, Japan). Cytospin samples and tissue sections were incubated with primary antibodies under the conditions listed in Table 1. As a second or third application, biotinylated donkey anti-rabbit IgG (Amersham, Japan), Alexafluor 568-labeled goat anti-rabbit IgG (Molecular Probe, USA), fluorescein isothiocyanate-labeled sheep anti-rabbit IgG (Abcam, UK), Alexafluor 488-labeled donkey anti-rat IgG (Invitrogen, USA), donkey anti-goat IgG (Invitrogen, USA), biotinylated anti-mouse IgG (Rockland, Gilbertsville, Pennsylvania, USA), biotinylated anti-rabbit IgG (Amersham Place, Little Chalfont, Buckinghamshire, England), and avidin-Alexafluor 568 (Molecular Probe, USA) were used, as described previously (Matsuyama et al. 2001; Nakagaki and Taguchi 2005). Triple-color immunofluorescence analysis was also performed and avidin-RPE-Cy5.5 (SouthernBiotech, Birmingham, AL, USA). Briefly, cytospin samples and tissue sections were first washed in PBS and treated with 1% Triton X-100 (Sigma, Tokyo, Japan) in 50% normal horse serum (Invitrogen, USA) diluted in PBS for 15 minutes followed by the above-described primary antibodies for 90 minutes. After washing, samples were incubated with secondary antibodies for 60 minutes. Triple-color immunofluorescence analysis was also performed and avidin-RPE-Cy5.5 (Serotec, UK) was used as the third reagent. The double and triple-stained sections were examined using a fluorescence microscope (KEYENCE, Osaka, Japan) or confocal laser-scanning microscope (Leica Microsystems, Germany).

Neuropathology

The degree of spongiform neurodegeneration was scored as follows (Nakai et al. 2005) : 0, no lesions; 1, less than 20 vacuoles in the total area; 2, 20 to 100 vacuoles counted in the light microscopical field at 10x magnification (field (X10)); 3, clusters consisting of over 100 vacuoles spread within one field (X10); 4, more than two clusters consisting of over 100 vacuoles in the area, or clusters of vacuoles occupying over 30% of the total area. Intermediate scoring between each of the five established scores was permitted by adding a value of 0.5 to the lower score. To score the

CNS pathology, five areas were selected: the frontal hemisphere, thalamus, cerebellum, pons, and spinal cord.

The intensities of inflammation were scored separately either in the perivascular area (PVA) or in the parenchyma (BP) of the brain. Scoring was performed in five areas: cerebral cortex at the level of the parietal and frontal lobes, thalamus, pons, and spinal cord. The degree of inflammation in PVA was scored counting inflammatory cells located in the Virchow-Robin space, and as follows: 0: no inflammatory cells; 1: 5-10 cells and less than 4 blood vessels with inflammation in the sample area; 2: 10-30 cells and 5-9 blood vessels with inflammation in the sample area; 3: 10-19 blood vessels with inflammation in the sample area; 4: more than 20 blood vessels with inflammation in the sample area. Intermediate scoring in between each of the four established scores was permitted by adding a value of 0.5 to the lower score, which was also applied to the scoring for inflammation in the BP. Parenchymal inflammation in the brain was counted when the inflammation extended beyond the perivascular area, and was scored as follows: 0: no inflammatory cells; 1: 10-20 inflammatory cells in the sample area; 2: 30-50 inflammatory cells in the sample area; 3: more than 100 inflammatory cells in a restricted area involving less than 10% of the sample area; 4: more than one third of the sample area involved in inflammation.

Quantification of immunofluorescence staining brain parenchyma

Coronal sections of upper pons including superior cerebellar peduncle (scp) were analyzed by immunohistochemistry using anti-ER-TR7 and anti-Laminin antibodies. Fluorescence images of the brain from control and infected mice 12 and 48 hours after infection were used for quantification. All images had a resolution of $1,360 \times 1,024$ pixels with 256 intensity levels for each RGB component. The average fluorescence intensities (AFI) of ER-TR7 and laminin were measured in the same areas and quantitated by using a BZ-analyzer (Keyence, Osaka, Japan). As scp is not always present on both sides of upper pons, we measured the area of the region on one side of the brain where it was clearly visible. Immunohistochemical fluorescence intensities of parenchymal areas of pons were quantitatively measured. Normalized fluorescence intensity on each section was determined by subtracting the geometric mean fluorescence of either a dark image region or unstained areas.

In vitro stimulation of mouse splenic cells

Spleen cells were isolated from wt and mutant mice at 48 hours after injection of *srr7*, and from uninfected mice as the controls. Cells were washed with saline, and the erythrocytes were lysed using 0.83% NH_4Cl -Tris buffer (pH 7.65). Splenic cells were seeded at $2 \times 10^6/\text{ml}$ into wells of 24-well plates containing RPMI 1640 (Gibco) supplemented with 10% heat-inactivated FBS (Gibco). The cells were stimulated with the following stimulations: polyinosinic acid: polycytidylic acid (poly I:C) for Toll like receptor (TLR) 3 at $5\mu\text{g}/\text{ml}$; lipopolysaccharide (LPS) from *E. coli* for TLR4 at $5\mu\text{g}/\text{ml}$; single-stranded RNA (ssRNA) for TLR7 at $1\mu\text{g}/\text{ml}$; and Cytosine-phosphodiester-guanine (CpG) oligonucleotides for TLR9 at $5\mu\text{M}$. All TLR agonists

were purchased from InvivoGen (San Diego, CA, USA). Unstimulated cells were used as a negative control, and cells stimulated with concanavalin A (ConA, 1 µg/ml; Sigma) were the positive control for T-cell activation. The cells were then incubated at 37°C for 24 hours, and the supernatants were collected for cytokine analysis.

Tissue lysate preparation

The brains and spleens from uninfected and infected mice were quickly removed, placed on an ice-cold surface, and the hippocampus and pons were dissected. All tissues were snap-frozen and stored at -80 °C until processing. The frozen tissues were powdered by an SK-100 mill (Tokken Inc., Chiba, Japan). Protein was purified from dissected tissues in Radio-Immunoprecipitation Assay buffer (Wako, Osaka, Japan) and cell lysis buffer (Affimetrix, Santa Clara, CA, USA) supplemented with protease inhibitors (leupeptin, pepstatin, and chymostatin; Sigma, Tokyo, Japan). After centrifuged at 4°C and 14,000 rpm for 30 minutes, the supernatant was collected and stored at -80°C.

Detection of cytokines

Cytokines in the culture supernatant were assayed by a Luminex microbead-based multiplexed assay (Luminex Corp., Austin, TX, USA) using commercially available kits according to the manufacturer's protocol (Affimetrix, Santa Clara, CA, USA). Cytokines analyzed by the array include interferon (IFN)-β and monocyte chemoattractant protein 1 (MCP-1).

Statistical analysis

Overall survival was analyzed and compared by the Kaplan-Meier method. Differences in survival were tested for statistical significance by the log-rank test. Otherwise, the Student *t* test was used. P values of less than 0.05 were considered to indicate statistical significance.

3. Result

3-1. Neuropathologic feature of infection with srr7

A neuropathogenic JHM strain, srr7, was found to induce spongiform encephalopathy in the infected mice. The distinct vacuolar degeneration could be detectable at 48 hours pi in the area where no viral antigens were detected. In all of the neuropathologically examined animals, large extensive spongiotic lesions composed of various sizes of vacuole became apparent 4-5 days after viral inoculation mainly in the pons, cerebellum, and thalamus (Figure 1), and the lesions were less extensive in the frontal area (Figure 6O and P). The spongiosis exhibited several neuropathological characteristics. First, the lesion was fairly well-demarcated (Figure 2A and D). Second, the lesions were accompanied by few or no inflammatory reactions. This phenomenon occurs rather rarely in viral infections with apparent destructive lesions. At a lower magnification of extensive spongiotic lesion, many small nuclei were observed (Figure 2A), many of which were pycnotic and devoid of cytoplasm at a higher magnification (Figure 2B). We were unable to characterize the remainder, except for a few macrophages present in the lesions (black arrows in Figure 2B). Around the blood vessels in and around the extensive spongiotic lesion, almost no inflammatory cell exudation was observed neither at the capillary level nor at a larger size (thin white arrows in Figure 2A, C, and E). Occasionally, near the extensive spongiotic lesion, perivascular cell infiltration was observed (thin white arrow in Figure 2D). Interestingly, these exuded cells seemed stick together tightly in the of Virchow-Robin space, as if they could not undergo migration. The third neuropathological characteristic of extensive spongiotic lesion is that neurons looking viable were found in the lesion (white arrowheads in Figure 2A and B), where vacuoles attached to the neurons directly. The neurons were also well-preserved in vacuolar lesion around the extensive spongiotic lesion (Figure 2A and C). The viral antigens were more strongly expressed around the extensive spongiotic lesion than inside (Figure 2K and L). Although the initial viral antigen-expression is detected in the inflammatory cells in the meninges, as early as 12 hours p.i., followed by infection to the choroid plexus and ependymal cells, as reported previously (Takatsuki et al. 2010), they were eliminated from ependymal cells and the subventricular zone (SVZ) in the latter phase of infection (Figure 2K). In addition, facing the ventricles, a repaired line of ependymal cells with flattened cytoplasm and few cilia was observed (Figure 2G and H). Another trace of initial events could be detected as pronounced activation of GFAP-positive glial cells in and around the SVZ. The gliosis was found to extend deep into the brain parenchyma, and, again, in the middle of the extensive spongiotic lesion (black arrowheads in Figure 2I), GFAP-antigen expression was less extensive than that seen in the surrounding vacuolar lesion. Even in this area with mild gliosis, astroglial foot processes around the blood vessels were an outstanding feature (Figure 2J), indicating that the blood brain barrier had been well-preserved in the extensive spongiotic lesion during the course of the disease.

3-2. Viral distribution

We failed to prove the importance of other types of immuno-competent cell by obtaining double or triple stained pictures of immunofluorescence, probably due to technical reasons through

using paraffin-embedded or frozen sections, as is indicated in previous reports (Takatsuki et al. 2010). We employed a cytopspin procedure to collect and mount leukocytes on glass slides in order to achieve better preservation of the antigenicities of cell marker proteins and the cell architecture on immunofluorescent studies of infected cells (Kashiwazaki et al. 2011b). At 12 hours pi, we found infected cells both in the meninx and spleen. The CNS is an immune-privileged environment, yet the local control of multiple pathogens is dependent on the ability of immune cells to access and operate within this site. It is also apparent that cells of the immune system have access to meninx. In addition, we found part of infected cells observed in the meningeal space were CD11b or F4/80-positive monocyte lineage cells which plays an important role in innate immunity. These observations lead us to identify infected cells observed in the spleen which contains abundant immune cells.

Super acute spread (SAS), which was ascertained through the use of paraffin-embedded or frozen sections obtained from mice infected with cl-2 or srr7 viruses (Takatsuki et al. 2010), was also detected by means of immunostaining for splenic cells collected and attached to glass slides following the cytopspin procedure (Figure 3A). The number of infected cells observed in the subarachnoidal space was greater than that in the spleen. Therefore, it is a possibility that a few viral particles leak into the blood stream and reach the spleen at the time of infection. The cytopspin procedure is the method for collecting and mounting leukocytes on glass slides in order to achieve better preservation of the antigenicities of cell marker proteins and the cell architecture on immunofluorescent studies of infected cells. It was estimated that less than 0.1 or 0.3 % of the total splenic cells were infected with srr7 or cl-2 viruses at 12 hours pi, respectively (Figure 3B). SAS was further ascertained by the co-culture of splenic cells recovered from infected mice with MHV-susceptible DBT cells (Figure 3C). Around 1 or 50 cells per 1×10^8 splenic cells produced infectious viral particles at 12 hours pi with srr7 or cl-2 viruses, respectively. The infectivity (Figure 3B) and viral productivity (Figure 3C) of cl-2 were higher than those of srr7 at 12 hours pi, t values on Student's test were $p < 0.05$ and 0.01, respectively). By 24 hours pi, the viral productivity of srr7 in the spleen increased more than ten times, but did not catch up with that of cl-2 at 24 hours pi (Figure 3C).

As shown in Figure 4, all kinds of cell population investigated with double-colored immuno-fluorescence for viral antigens and for specific cell marker proteins of immuno-competent cells, such as F4/80 for macrophages (Figure 5A1), TCR for T cells (Figure 5A2), or CD20 for B cells (Figure 5A3), at every time point between 12 and 48 hours pi were infected. In addition, CD11c-positive cells (Figure 5A4), especially highly marked and large-sized cells, which are considered to be conventional dendritic cells (cDCs), were verified to be infected. The targets of infection included Gr-1-positive cells and Ly-6C-positive cells (Figure 5A5 and A7, respectively) and B220⁻Ly-6C⁺ polynuclear cells (Figure 5B). Many B220⁺ cells were also infected (Figure 5A6). B220⁺Ly-6C⁺JHM⁺ cells were found in the spleen during early phase of infection (Figure 5B and C). We were able to prove that plasmacytoid dendritic cells (pDCs) were infected with our viruses during the initial phase of infection by a cytopspin procedure.

Surprisingly, at 48 hours pi, we found large vacuolar lesions where viral antigens were not detected (Figure 6A–G). To study vacuolar formation during the early phase of infection, we investigated infected mice at 48 hours pi, because the viral antigens are distributed only in the restricted area (Takatsuki et al. 2010) at this time while vacuolar lesion became apparent (Figure 6B, F and G). Vacuolar degeneration was already detectable before 48 hours pi, but the number of vacuoles and magnitude were so low that it was sometimes difficult to distinguish from an artifact produced during the preparation of sections (data not shown). In the dotted area with the letter B, a distinct vacuolar lesion developed (Figure 6B), but viral antigens were not detectable both in this area and in the area between the dotted area and ependymal cells which expressed the viral antigens. Occasionally viral antigen-bearing cells in the SVZ were observed extending their cytoplasm to the ventricle (Figure 6C). We considered these to be B cells, GFAP-positive precursor cells resident in the SVZ, so we carried out double staining of serial sections next to the stained section (Figure 6C). As shown in Figure 6E, a GFAP-positive cell projecting its cytoplasm to the ventricular surface was infected.

Astroglial activations were most prominent in the area near the very restricted site of infection around the ventricle, and already during this early stage of infection, gliosis was found extending deep into the brain parenchyma, like in the later stage but in a less extensive manner (Figure 6D). Interestingly, in the cerebellum, the area of gliosis abruptly ended at the border of the granular layer (indicated by black arrowheads in Figure 6D and F). Similarly, the vacuolar lesion finished there. At a lower magnification, the activated astrocytes looked scattered and unrelated to the vacuoles observed in the region of gliosis (Figure 6F), but a higher magnification revealed that fine fibrous or dot-like structures exhibiting GFAP-antigens were facing the vacuolar walls (Figure 6G). A similar distribution of viral antigens, gliosis, and vacuolar degeneration was observed at various levels around the third (IIIv) or lateral (LV) ventricles (Figure 6H–P). Although viral infection and glial reactions were observed around the LV in the frontal portion (Figure 6N), spongiosis did not become prominent around this area (Figure 6O and P). Additional viral infection outside the SVZ was observed in the white matter near the ventricle, namely in the corpus callosum (white arrowheads in Figure 6H and I). These infected cells did not look as if they appeared as a consequence of the direct spread of viruses from the IIIv or LV, but the staining of serial sections showed that the viral antigens were distributed from the junctional area between the meninx, choroid plexus, and LV to the surrounding white matter (Figure 6R and S). Another viral infection outside the SVZ was detected as an occasional and solitary infection in the thalamus and basal ganglia during this early stage of infection (Figure 6Q). This type of infection was not accompanied by a prominent astroglial reaction nor vacuolar lesion in the surroundings. On the 3 days pi, the distributions of viral antigens not continuous with the antigen spread around the SVZ became more prominent (Figure 6T).

There is no marker specific for type B cells at present. GFAP is one of the antigens which type B cells express, but astrocytes also express GFAP. It is not certain that these type B cells which we considered are, in fact, astrocytes. However, type B cells have different molecular features,

because they express nestin (an intermediate filament), that characterise only embryonic astrocytes, reactive astrocytes or neuroblasts and intermediate progenitors. Viral antigens were detected in the nestin-positive immature cells beneath the ependymal cells at 48 hours pi when spongiosis became apparent in which lesions no viral antigens were detectable. We demonstrated that nestin-positive precursor cells in the SVZ were also infected (Figure 6U). This infected progenitor cells were also observed in cl-2 infected mice. We successfully identified infected type B cells in the SVZ during initial phase of infection.

3-3. Cytokine production

As previous studies reported that the FRN maturation required the expression of cytokines, indicating that cytokine production in the brain might be different between cl-2 and srr7. The production of cytokines in the brain was examined. In the pons, IFN- β , interleukin (IL)-1 β , IL-6, MCP-1, and tumor necrosis factor (TNF)- α levels were strongly elevated after infection (Figure. 7A). These cytokines were induced in neurons and astrocytes (Figure 7B). There was significant difference in cytokine levels between these two strains. High levels of circulating IFN- β , IL-1 β , IL-6, MCP-1, and TNF- α were detected in the brain of mice infected with cl-2.

3-4. Induction of the components of FRN after infection

To visualize cells of the reticular network, we used anti- ER-TR7 (Van Vliet et al. 1986) and anti-laminin antibodies, which stain the FRN in the white pulp and red pulp in the spleen (Figure 8A). Viral antigens are detected in the cytoplasm of the cells, where viruses replicate. However, we found viral antigens in the meninges, where viral antigens were colocalized with fibrous extracellular matrix (Figure 8B and C). In the parenchyma of the pons, the colocalization was also found around large blood vessel (Figure 8D). The FRN is thought to play numerous roles in lymphoid organs, influencing cell recruitment, migration, activation, and survival through organization of the lymphoid cellular and molecular microarchitecture. The FRN form a contiguous network of conduits that allow transport of small molecules and antigens (Gretz et al. 2000). Therefore, we examined whether ER-TR7-positive fibrous structure in the brain functions by way of intravenous injection of fluorescent-labeled dextran. In the spleen, this fluorescent tracer colocalized with ER-TR7 as reported previously (Figure 9A and B). Texas Red-conjugated dextran was clearly observed in the conduits of the spleen 10 minutes after injection. In the brain, the tracer was found to migrate into the choroid plexus (Figure 9C), but this migration was not detected in the brain of uninfected mice (data not shown). This suggested that high molecular weight foreign substances require high expression of ER-TR7 to enter this area. Judging from the localization of dextran, it is possible that antigens or viral particles in the subarachnoid space pass into the choroid plexus guided by ER-TR7-positive fibers through the junctional area between the fourth ventricle and meninx around the foramen of Luschka. These results suggested that viral antigen-positive fibrous structure, colocalized with ER-TR7 and laminin, must be FRN-like structure which promotes trafficking antigens in these distinct compartments of the brain.

3-5. Inductin of the components of FRN after viral infection

In the brain of the uninfected mice, both ER-TR7 and laminin were expressed at low basal amounts in uninfected brains and it was restricted to blood vessels and meninges. In infected mice, there was increased ER-TR7 staining, and ER-TR7-positive fibrous structure was detected in the parenchyma at 48 hours pi, which was not detected in the uninfected brain (Figure 10). Interestingly, increased ER-TR7 expression after infection was observed not only in the fibrous structures but also in the cytoplasm of cell components in the central nervous system. Therefore, we performed a detailed characterization of ER-TR7⁺Laminin⁻ cell subsets in vivo and in vitro. ER-TR7 was detected in the Zic-2 or cytokeratin-positive arachnoid cells in the meninges and ependymal cell layer (Figure 11A and B). Furthermore, at 48 hours pi, ER-TR7 antigen was detected in GFAP-positive astrocytes (Figure 11C), and NeuN-positive neurons (Figure 11D) in the brain. We also found ER-TR7 expression in oligodendrocytes in the white matter in the parenchymal area (Figure 11E). The existence of ER-TR7 positive cellular component in the central nervous system was confirmed in primary culture from brain. As expected, cultured cells were double-immunolabeled for ER-TR7 and Olig2 (oligodendrocyte transcription factor 2) or neurofilament (NF) (Figure 11F).

We also found ER-TR7 antigen expression without an association with ECM components including laminin (Figure 10). A possible explanation of this observation is that immature ER-TR7 antigen-positive fibers may be formed during the initial stages of the host reaction, compared to the mature form of ER-TR7 antigen-positive reticular fibers associated with ECM structures, as is observed in the lymphoid organs. When we compared the length of ER-TR7-positive fibers colocalized with laminin in the ventricle of cl-2 and sham-inoculated mice, we found a greater difference in the two groups (Figure 12) than in comparisons of ER-TR7-positive fibers alone.

3-6. Overproduction of inflammatory mediators contributes to the pathogenesis

α 1,3-fucosyltransferase 9 knockout (Fut9^{-/-}) mice are unable to synthesize the Lewis x (Le^x) structure, because Le^x and Fut9 are highly expressed in the central nervous system (CNS). In addition, Fut9^{-/-} mice develop normally without gross phenotypic abnormalities in the brain and other organs (Kudo et al. 2004), which might affect pathological changes induced by viral infection.

In order to study the host response to foreign invasion in Fut9^{-/-} mice, we infected the mice with highly neuropathogenic viruses, srr7 which induces pathological lesions in the CNS, spleen, and liver with a short incubation period. No fundamental differences among different strains of mice after infection either with srr7 were observed (Figure 13A, $p > 0.05$ with the Kaplan-Meier method), showing that infected mice died within 10 days pi when inoculated with srr7. Viral titers prepared from organs of infected mice at desired time points are shown in Figure 13B. The viral growth was compared among Fut9^{-/-} with a genetic background of BALB/c and BALB/c mice. Viral growth in Fut9^{-/-} mice was markedly lower after 48 hours pi compared with that in wild-type mice (Figure 13B). Viral growth in Fut9^{-/-} was slower than that in the wild-type mice.

Pathological pictures were compared between those obtained from wild-type and Fut9^{-/-} mice infected with srr7 virus (Figure 14A-D). A significant difference was observed in parenchymal inflammation at 6 days pi after scoring the inflammatory intensities in the infected brain. A prominent inflammation extending to the brain parenchyma was observed in infected Fut9^{-/-} mice (Figure 14A and B). At 48 hours pi, cell infiltration beyond the Virchow-Robin space was often observed in the infected brain parenchyma of Fut9^{-/-} mice.

There were almost no differences between mutant and wild-type mice in the shift of cytokine levels after infection examined in the pons and spleen, except for IFN- β in the pons, and INF- γ , IL-6 and MCP-1 in the spleen (Figure 15A). IFN- β production in the pons obtained from Fut9^{-/-} mice was comparable with that in cl-2-infected mice (Figure 15B). The producibility of cytokines in vitro by cultured splenic leukocytes was also examined (Figure 16), using Poly I:C, LPS, ssRNA, CpG, and ConA, which are representative stimulator for Toll like receptor (TLR) 3, 4, 7, 9, and T-lymphocytes, respectively (Blasius et al. 2010; Mazaleuskaya et al. 2012). Reduction in IFN- β production by splenic cells (Spc) obtained from infected wild-type and mutant mice ((v+)/Wt and (v+)/Fut^{-/-}, respectively) compared to those from uninfected (v-) mice was observed after stimulation using LPS or ConA, both of which exert stimulative effects after binding cell surface structure. A striking difference between SpcWt and Fut9^{-/-} was detected in MCP-1 producibility of Spc. The amount of MCP-1 measured in the supernatant of Spc(v+)Wt culture were much lower (P<0.05) compared to those of Spc(v-)Wt culture after stimulation with LPS, ssRNA, and ConA, whereas the reduction was not observed by CpG stimulation. In contrast, Spc(+) and (-) of Fut9^{-/-} did not show differences in MCP-1-producibility after cell culture with any of the stimulators examined (Figure 16).

4. Discussion

The possible mechanisms of pathogenesis

The initial phase of infection with cl-2 and srr7 during 12 and 48 hours pi showed that there were no significant differences among the two viruses in the population of infected cells which appeared in brain and spleen. Initial viral antigens were detected at 12 hours pi in the infiltrating cells that appeared in the subarachnoidal space of mouse brains infected with the viruses. There were no significant differences in the intensity or spread of viral antigens in the inflammatory cells between the two viruses. These antigen-positive cells appeared in the subarachnoidal space prior to viral spread into the brain parenchyma, indicating that viral encephalitis starts with infection of the infiltrating monocyte lineage which expresses MHVR.

Both cl-2 and srr7 induce syncytium formation in the infiltrating cells in the subarachnoidal space (Takatsuki et al. 2010). The appearance of syncytium formation in circulating leukocytes indicates that the viruses are able to induce direct cytopathic effects on the infected immuno-competent cells, leading to a rapid spread of the viruses during a very early phase of infection, overcoming the innate immunity of hosts, which is induced at the earliest step of viral infection through the recognition of viral components by host pattern-recognition receptors such as the Toll-like receptor family. IFN receptor expression in monocyte lineage or dendritic cells can play a primary role in the early containment of MHV, in addition to the role of IFN production in infected tissue. During this time, the host's adaptive immune reaction against the virus has yet to be initiated, which mediates protection from lethal coronavirus encephalomyelitis caused by other JHM strains of MHV after propagating a successful innate immune response, owing much to type I IFN production. In contrast, infection with srr7, which spreads in a receptor (CEACAM1a)-dependent manner, does not induce such a rapid death of infected mice, in the absence of infecting critical targets, such as neurons, in the CNS. Nevertheless, srr7, which differs only in one amino acid sequence in the S region, successfully propagates in the CNS, shown by the compatible viral growth compared with cl-2 determined by a titration assay.

We also demonstrated varied cell populations infected with cl-2 or srr7 corresponding to variable cell populations including pDCs which express MHVR during the early phase of infection, indicating that there was no significant difference in the viral growth between two strains. Activated pDCs produce proinflammatory cytokines, such as type I IFNs, in large quantities, which are particularly important in resistance to virus infection. Recently it was reported that standard populations of pDCs isolated through the use of monoclonal antibodies contain a subtype IFN-producing killer dendritic cells, with distinct functions. We also identified a morphologically heterogeneous population among B220⁺Ly-6C⁺ cells in smeared samples on glass slides after isolation with a cell sorter (data not shown), and in the cytopspin procedure, including small-sized and multinucleated cells, which are distinct from the typical morphological pictures of pDCs initially reported. In addition to the further characterization of B220⁺Ly-6C⁺ cells after virus infection, the possibility that migrating pDCs might be infected at the site of initial infection is being examined in our laboratory employing whole mounting of freshly isolated meninges from

infected mice, which would overcome the technical difficulty of identifying infected cells through the use of frozen or paraffin-embedded materials. In conclusion, *srr7* as well as *cl-2* infection could have induced a rapid viral spread in the infected CNS after effectively suppressing initial innate immunity through inducing cytopathic effects on the infected immuno-competent infiltrating cells and infecting pDCs during the initial phase of infection.

In the case of *srr7* infection, the distribution of extensive spongiotic lesions showed a predilection for the brainstem and cerebellum, and the viral antigens in the brain appear in the choroid plexus and SVZ including ependymal cells during the early phase of infection after the initial emergence in infiltrating cells of meninges at 12 hours pi (Takatsuki et al. 2010). Therefore, our studies on the relation between the viral antigen distribution and formation of vacuolar degeneration were mainly focused on the periventricular and the surrounding areas in the brainstem. Surprisingly, at 48 hours pi, we found large vacuolar lesion where viral antigens were not detected. On the same section as the vacuolar lesion were detected or on successive serial sections, viral antigens were found only in restricted areas, i.e., the SVZ, where GFAP-positive cells with a peculiar shape, projecting narrow cytoplasm to the ventricular surface and leaving their perikaryon beneath the surface-lining ependymal cells, were found to have been infected. The shape and localization of these astrocytes corresponded to B (Alvarez-Buylla and Lim 2004) or B1 (Mirzadeh et al. 2008) cells, which serve as both stem and niche cells in the SVZ and play critical roles in adult neurogenesis. B cells bear GFAP and have a long basal process that terminates on blood vessels and an apical ending at the ventricle surface, with long cilia projecting into the ventricle (Alvarez-Buylla and Lim 2004), which can be a target of infection via infected monocytes that have infiltrated the ventricle during the initial phase of infection (Takatsuki et al. 2010). It is not plausible for the infected GFAP-positive cells in the SVZ to have a direct effect on spongiosis, at least in the area around the third ventricle shown, because the vacuolar lesion was located a long way from the SVZ. Instead, these cells might have triggered a chain reaction of astrogliosis which spread from the SVZ reaching the deep white matter of the cerebellum through the pathway of neurogenesis or the blood supply, because inquiringly this area of gliosis ended abruptly at the edge of the granular layer. It is presumed that B cell-originating migratory cells ascend in close contact with the basal lamina along with blood vessels in adulthood (Mirzadeh et al. 2008). The cerebellar cortex receives its blood supply from the meninges that cover the cerebellum, in a different way from the cerebellar white matter. In addition, the granular layer is formed from granular neurons that have migrated from the external granular layer during embryonic and postnatal stages in mice (Goldowitz and Hamre 1998). Those activated astrocytes in a large area after being triggered by infection of the SVZ must have communicated with each other, leading to vacuolar formation away from the infection sites. This cell-to-cell communication can be facilitated by direct contact with each other through an elongated cytoplasmic projection as reported for the immunological synapse between leukocytes, especially between dendritic cells and lymphocytes (Lee et al. 2002). Fine projections of astrocytes are detected in vacuolar lesion, where, at a higher magnification, GFAP-positive foot processes were shown to be closely attached to the vacuolar walls. Type B cells

have been considered as “nursing cells” capable of maintaining the extracellular homeostasis and providing metabolic support for the neuronal functioning. Infection could alter this important role of type B cells for neurons, inducing neuronal degeneration.

Contribution of cytokines to pathogenesis

Signals can be spread by means of cytokine production, which is observed in all kinds of cell constituting the CNS, including astrocytes and neurons (McMenamin et al. 1999). The contribution of microglia (Minghetti et al. 2005) in this context should not be ignored, but the activation of microglia monitored by F4/80 or CD11b expression was not prominent at 48 hours pi. Furthermore, it has been reported that neurodegenerative progression can be protected by microglia and monocyte lineages, which produce neurotrophins (Nakajima et al. 2001).

We found the IFN- β , MCP-1 or IL-1 β -positive neuronal cells including neurons and astrocytes in the brain parenchyma during infection. These cytokine productions during the early phase of infection in the brain were greater in cl-2-infected mice compared with that in srr7-infected mice, leading to the difference in neuropathogenesis between two strains. In agreement with previous reports (Rostène et al. 2007), we detected cytokine expression in cell components of the CNS including astrocytes and neurons. In the brain, foot processes of astrocytes, neurons and microglia adhere to the basement lamina around the blood vessels. An important question is how signals that reach the cells around the blood vessels are then transmitted further. Two possibilities might be cell-to-cell-mediated immune cross-talk through an immune synapse, as reported in the lymphoid cells, or the use of immune-related molecules and several neurotransmitters as a tool. In this way, it might trigger an immune reaction in the brain parenchymal cells. Astrocytes may play such a role in cellular communication because a GFAP-positive fibrous network was connected to cytokine-producing cells and ER-TR7-positive fibers distributed in wide parenchymal area. We suggested that the central nervous system employs a unique conduit system for immune communication. In this immune communication network, there might be differences between cl-2 and srr7, leading to different neuropathogenesis. We are studying the expression of ER-TR7 antigen in the brain of srr7-infected mice to confirm whether the maturation of reticular network is different from that in cl-2.

The contribution of cytokines to neuropathogenesis is supported by the result of the pathological change in Fut9^{-/-} mice. It is indicated that the fulminant inflammation observed in the brain of mutant mice might have induced more lethal effects on infected mutant mice than direct virus-induced destructive changes in the brain, leading to a similar survival rate as in wild-type mice in spite of the markedly lower viral proliferation in the Fut9^{-/-} mice after infection. Proinflammatory cytokines might play important roles not only in different aspects of animal health but also in a participant in degenerative events. We found the MCP-1 or IL-1 β -positive neuronal cells in the brain parenchyma during infection. These anti-viral mechanisms during the initial phase of infection have often been discussed and categorized in innate immunity. However, the term “innate immunity” refers to a wide spectrum of early steps in immune reactions

such as cell-cell interaction mediated by proinflammatory cytokines or even an arrangement for adaptive immunity in a primary stage. Because of the marked disagreement between viral infectivity and producibility observed in the wild-type and mutant mice using our viruses, we refer to the occurrences in target cells that eliminate viruses or prevent viral maturation after infection as intracellular immunity to distinguish from so-called “innate immunity”, to make our discussion points clear. Our results indicate the over-production of cytokines in the mutant mice after infection. When the immune response is excessive, it can exacerbate the infection and result in a poor clinical outcome which is evident in disease caused by influenza virus infection (Kobasa et al. 2007). An aberrant innate immune response after infection with the over-production of cytokines, failure to eliminate infectious agents, and resultant morbidity and mortality, which is designated as a cytokine storm (Taubenberger et al. 2008) can be regulated by the inhibitory cascade. A sphingolipid metabolite, sphingosine-1 phosphate (S1P), and S1P receptor mediate inhibition of the innate immune response (Walsh et al. 2011).

With the characteristic neuropathology of spongiosis where inflammatory cell infiltration was suppressed to the minimum level both in the initial phase and during the latter phase like in other extensive spongiotic lesions induced by different kinds of infectious agents (Crozet et al. 2008; Watanabe and Takase-Yoden 2006), *srr7* infection of mice would provide a superior experimental model to investigate the mechanism of how extensive spongiotic lesions are formed, which remains unclear in spite of the long history of scientific research since infectious spongiotic encephalopathy was first reported because of its extremely short incubation period compared with other experimental models of infectious spongiform degeneration in brains, minimizing many events inevitably induced after infection.

5. References

- Alvarez-Buylla A, Lim DA (2004) For the long run: Maintaining germinal niches in the adult brain. *Neuron* 41:683-686
- Bajénoff M, Glaichenhaus N, Germain RN (2008) Fibroblastic reticular cells guide T lymphocyte entry into and migration within the splenic T cell zone. *J Immunol* 181:3947-3954
- Beauchemin N, Draber P, Dveksler G, Gold P, Gray-Owen S, Grunert F, Hammarström S, Holmes K, Karlsson A, Kuroki M, Lin S, Lucka L, Najjar S, Neumaier M, Obrink B, Shively J, Skubitz K, Stanners C, Thomas P, Thompson J, Virji M, von Kleist S, Wagener C, Watt S, Zimmermann W (1999) Redefined nomenclature for members of the carcinoembryonic antigen family. *Exp Cell Res* 252:243-249
- Blasius AL, Beutler B (2010) Intracellular toll-like receptors. *Immunity* 32:305-315
- Chen D, Asanaka M, Yokomori K, Wang F, Hwang S, Li H, Lai M (1995) A pregnancy-specific glycoprotein is expressed in the brain and serves as a receptor for mouse hepatitis virus. *Proc Natl Acad Sci U S A* 92:12095-12099
- Crozet C, Beranger F, Lehmann S (2008) Cellular pathogenesis in prion diseases. *Vet Res* 39:44
- de Groot RJ, Luytjes W, Horzinek MC, van der Zeijst BA, Spaan WJ, Lenstra JA (1987) Evidence for a coiled-coil structure in the spike proteins of coronaviruses. *J Mol Biol* 196:963-966
- Egen JG, Rothfuchs AG, Feng CG, Winter N, Sher A, Germain RN (2008) Macrophage and T cell dynamics during the development and disintegration of mycobacterial granulomas. *Immunity* 28:271-284
- Gallagher TM, Buchmeier MJ, Perlman S (1992) Cell receptor-independent infection by a neurotropic murine coronavirus. *Virology* 191:517-522
- Godfraind C, Langreth S, Cardellicchio C, Knobler R, Coutelier J, Dubois-Dalcq M, Holmes K (1995) Tissue and cellular distribution of an adhesion molecule in the carcinoembryonic antigen family that serves as a receptor for mouse hepatitis virus. *Lab Invest* 73:615-627
- Goldowitz D, Hamre K (1998) The cells and molecules that make a cerebellum. *Trends Neurosci* 21:375-382
- Greicius G, Severinson E, Beauchemin N, Obrink B, Singer B (2003) CEACAM1 is a potent

regulator of B cell receptor complex-induced activation. *J Leukoc Biol* 74:126-134

Gretz JE, Norbury CC, Anderson AO, Proudfoot AE, Shaw S (2000) Lymph-borne chemokines and other low molecular weight molecules reach high endothelial venules via specialized conduits while a functional barrier limits access to the lymphocyte microenvironments in lymph node cortex. *J Exp Med* 192:1425-1440

Kammerer R, Stober D, Singer BB, Obrink B, Reimann J (2001) Carcinoembryonic antigen-related cell adhesion molecule 1 on murine dendritic cells is a potent regulator of T cell stimulation. *J Immunol* 166:6537-6544

Kashiwazaki H, Nomura R, Matsuyama S, Taguchi F, Watanabe R (2011a) Spongiform degeneration induced by neuropathogenic murine coronavirus infection. *Pathol Int* 61:184-191

Kashiwazaki H, Taguchi F, Ikehara Y, Watanabe R (2011b) Characterization of splenic cells during the early phase of infection with neuropathogenic mouse hepatitis virus. *Jpn J Infect Dis* 64:256-259

Kobasa D, Jones SM, Shinya K, Kash JC, Copps J, Ebihara H, Hatta Y, Kim JH, Halfmann P, Hatta M, Feldmann F, Alimonti JB, Fernando L, Li Y, Katze MG, Feldmann H, Kawaoka Y (2007) Aberrant innate immune response in lethal infection of macaques with the 1918 influenza virus. *Nature* 445:319-323

Kudo T, Fujii T, Ikegami S, Inokuchi K, Takayama Y, Ikehara Y, Nishihara S, Togayachi A, Takahashi S, Tachibana K, Yuasa S, Narimatsu H (2007) Mice lacking alpha1,3-fucosyltransferase IX demonstrate disappearance of Lewis x structure in brain and increased anxiety-like behaviors. *Glycobiology* 17:1-9

Kudo T, Kaneko M, Iwasaki H, Togayachi A, Nishihara S, Abe K, Narimatsu H (2004) Normal embryonic and germ cell development in mice lacking alpha 1,3-fucosyltransferase IX (Fut9) which show disappearance of stage-specific embryonic antigen 1. *Mol Cell Biol* 24:4221-4228

Lee SJE, Hori Y, Groves JT, Dustin ML, Chakraborty AK (2002) Correlation of a dynamic model for immunological synapse formation with effector functions: two pathways to synapse formation. *Trends in Immunology* 23:492-499

Matsuyama S, Watanabe R, Taguchi F (2001) Neurovirulence in mice of soluble receptor-resistant (srr) mutants of mouse hepatitis virus: intensive apoptosis caused by less virulent srr mutant. *Arch Virol* 146:1643-1654

Mazaleuskaya L, Veltrop R, Ikpeze N, Martin-Garcia J, Navas-Martin S (2012) Protective role of Toll-like Receptor 3-induced type I interferon in murine coronavirus infection of macrophages. *Viruses* 4:901-923

McMenamin PG (1999) Distribution and phenotype of dendritic cells and resident tissue macrophages in the dura mater, leptomeninges, and choroid plexus of the rat brain as demonstrated in wholemount preparations. *J Comp Neurol* 405:553-562

Minghetti L, Ajmone-Cat MA, De Bernardinis MA, De Simone R (2005) Microglial activation in chronic neurodegenerative diseases: roles of apoptotic neurons and chronic stimulation. *Brain Res Brain Res Rev* 48:251-256

Mirzadeh Z, Merkle FT, Soriano-Navarro M, Garcia-Verdugo JM, Alvarez-Buylla A (2008) Neural stem cells confer unique pinwheel architecture to the ventricular surface in neurogenic regions of the adult brain. *Cell Stem Cell* 3:265-278

Moller MJ, Kammerer R, Grunert F, von Kleist S (1996) Biliary glycoprotein (BGP) expression on T cells and on a natural-killer-cell sub-population. *Int J Cancer* 65:740-745

Mrass P, Takano H, Ng LG, Daxini S, Lasaro MO, Iparraguirre A, Cavanagh LL, von Andrian UH, Ertl HC, Haydon PG, Weninger W (2006) Random migration precedes stable target cell interactions of tumor-infiltrating T cells. *J Exp Med* 203:2749-2761

Mrass P, Weninger W (2006) Immune cell migration as a means to control immune privilege: lessons from the CNS and tumors. *Immunol Rev* 213:195-212

Mueller SN, Matloubian M, Clemens DM, Sharpe AH, Freeman GJ, Gangappa S, Larsen CP, Ahmed R (2007) Viral targeting of fibroblastic reticular cells contributes to immunosuppression and persistence during chronic infection. *Proc Natl Acad Sci U S A* 104:15430-15435

Nédellec P, Dveksler G, Daniels E, Turbide C, Chow B, Basile A, Holmes K, Beauchemin N (1994) Bgp2, a new member of the carcinoembryonic antigen-related gene family, encodes an alternative receptor for mouse hepatitis viruses. *J Virol* 68:4525-4537

Nakagaki K, Nakagaki K, Taguchi F (2005) Receptor-independent spread of a highly neurotropic murine coronavirus JHMV strain from initially infected microglial cells in mixed neural cultures. *J Virol* 79:6102-6110

- Nakai R, Takase-Yoden S, Watanabe R (2005) Analysis of the distribution of neuropathogenic retroviral antigens following PVC211 or A8-V infection. *Microbiol Immunol* 49:1075-1081
- Nakajima K, Honda S, Tohyama Y, Imai Y, Kohsaka S, Kurihara T (2001) Neurotrophin secretion from cultured microglia. *J Neurosci Res* 65:322-331
- Nolte MA, Belien JA, Schadee-Eestermans I, Jansen W, Unger WW, van Rooijen N, Kraal G, Mebius RE (2003) A conduit system distributes chemokines and small blood-borne molecules through the splenic white pulp. *J Exp Med* 198:505-512
- Odin P, Asplund M, Busch C, Obrink B (1988) Immunohistochemical localization of cellCAM 105 in rat tissues: appearance in epithelia, platelets, and granulocytes. *J Histochem Cytochem* 36:729-739
- Ohtsuka N, Yamada Y, Taguchi F (1996) Difference in virus-binding activity of two distinct receptor proteins for mouse hepatitis virus. *J Gen Virol* 77 (Pt 8):1683-1692
- Rao P, Kumari S, Gallagher T (1997) Identification of a contiguous 6-residue determinant in the MHV receptor that controls the level of virion binding to cells. *Virology* 229:336-348
- Rostène W, Kitabgi P, Parsadaniantz SM (2007) Chemokines: a new class of neuromodulator? *Nat Rev Neurosci* 8:895-903
- Saeki K, Ohtsuka N, Taguchi F (1997) Identification of spike protein residues of murine coronavirus responsible for receptor-binding activity by use of soluble receptor-resistant mutants. *J Virol* 71:9024-9031
- Steele KE, Anderson AO, Mohamadzadeh M (2009) Fibroblastic reticular cell infection by hemorrhagic fever viruses. *Immunotherapy* 1:187-197
- Sturman LS, Ricard CS, Holmes KV (1985) Proteolytic cleavage of the E2 glycoprotein of murine coronavirus: activation of cell-fusing activity of virions by trypsin and separation of two different 90K cleavage fragments. *J Virol* 56:904-911
- Taguchi F, Matsuyama S (2002) Soluble receptor potentiates receptor-independent infection by murine coronavirus. *J Virol* 76:950-958
- Taguchi F, Siddell SG, Wege H, ter Meulen V (1985) Characterization of a variant virus selected in rat brains after infection by coronavirus mouse hepatitis virus JHM. *J Virol* 54:429-435

Takatsuki H, Taguchi F, Nomura R, Kashiwazaki H, Watanabe M, Ikehara Y, Watanabe R (2010) Cytopathy of an infiltrating monocyte lineage during the early phase of infection with murine coronavirus in the brain. *Neuropathology* 30:361-371

Taubenberger JK, Morens DM (2008) The pathology of influenza virus infections. *Annu Rev Pathol* 3:499-522

Van Vliet E, Melis M, Foidart JM, Van Ewijk W (1986) Reticular fibroblasts in peripheral lymphoid organs identified by a monoclonal antibody. *J Histochem Cytochem* 34:883-890

Walsh KB, Teijaro JR, Rosen H, Oldstone MB (2011) Quelling the storm: utilization of sphingosine-1-phosphate receptor signaling to ameliorate influenza virus-induced cytokine storm. *Immunol Res* 51:15-25

Watanabe R, Takase-Yoden S (2006) Neuropathology induced by infection with Friend murine leukemia viral clone A8-V depends upon the level of viral antigen expression. *Neuropathology* 26:188-195

Wilson EH, Harris TH, Mrass P, John B, Tait ED, Wu GF, Pepper M, Wherry EJ, Dzierzinski F, Roos D, Haydon PG, Laufer TM, Weninger W, Hunter CA (2009) Behavior of parasite-specific effector CD8⁺ T cells in the brain and visualization of a kinesis-associated system of reticular fibers. *Immunity* 30:300-311

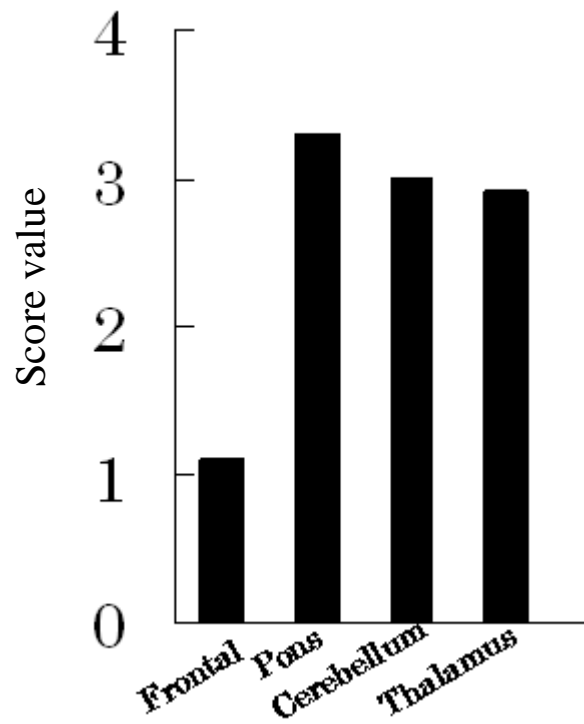


Figure 1 Neuropathological scores of spongiosis

The intensity of spongiosis was indicated as averaged scores in the frontal hemisphere (Frontal), pons, and cerebellum, obtained from examined animals.

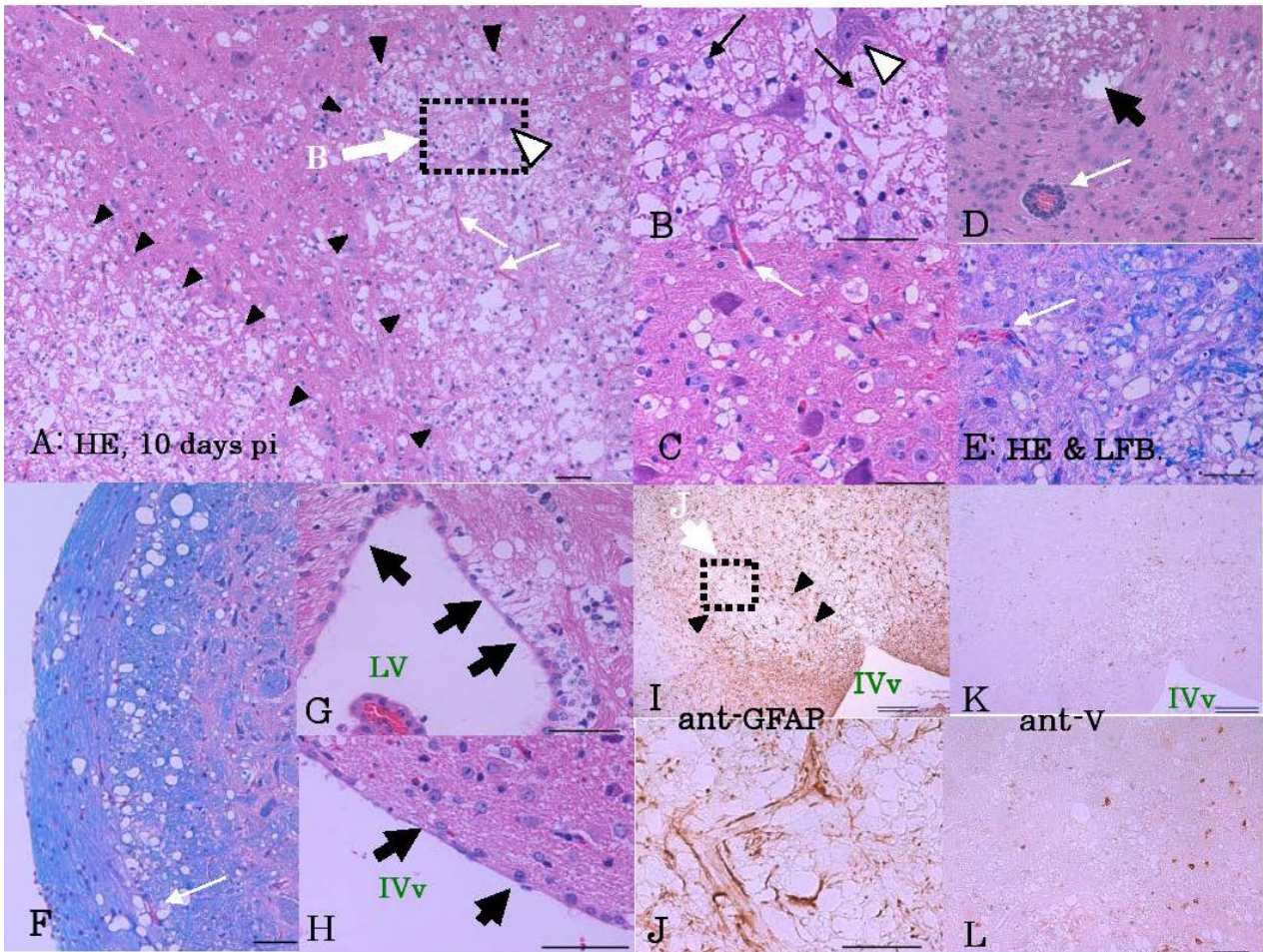


Figure 2 Spongiosis induced by *srr7*-infection

Paraffin-embedded coronal sections at the level of the middle pons (A-F, H-L) and infundibulum (G) were prepared from the brains of mice infected with *srr7* at 10 days pi, and were stained with HE (A-D, G-H) or HE and LFB (E, F). (A) Extensive areas of spongiosis (exSpongi) in the pons are marked by black arrowheads. The vacuolar degeneration observed in this picture was scored as grade 4 spongiosis (see Materials and Method). Around these areas, less extensive but distinct lesions with vacuolar degeneration (vacLesions) extend. Grossly normal neurons remain in the middle of exSpongi (white arrowhead), shown at a higher magnification in B. (B) Higher magnification of the dotted area in A (thick white arrow). Macrophages are indicated by black arrows. (C) The vacLesion around the exSpongi. (D) Perivascular cell infiltration (thin white arrow) was occasionally noted near the exSpongi (arrowheads). (E) Spongiosis involving an area with myelinated fibers. No macrophages are present. Around the blood vessel (thin white arrow), almost no infiltrated cells are seen. Thin white arrows in A and C point to small blood vessels of capillary size, and those in D-F indicate larger-sized blood vessels. (F) The vacLesion extended to the dorsal spinocerebellar tract. Macrophages or infiltrated cells around the blood vessels (thin white arrow) are not apparent. (G, H) Ependymal cells facing the lateral ventricle (LV), and the fourth ventricle (IVv) are attenuated (thick arrows) with less cilia. The ventricles are dilated. (I-L)

Immuno-histochemical staining of serial sections to detect GFAP (I, J) and the viral antigens (K, L), illustrated in the pictures as ant-GFAP and ant-V, respectively. Glial reactions are prominent around the ventricle and less extensive in the exSpongi (marked by black arrowheads). (J) illustrates a higher magnification of the dotted area in I to show, in the middle of exSpongi, astrocyte-foot processes are well preserved around the blood vessel, although the glial reaction is not as prominent as in the SVZ or surrounding vacLesions. The viral antigen distribution is also less prominent in exSpongi than in the surrounding area. Note that the viral antigens are not detectable in ependymal cells or in the SVZ facing the fourth ventricle (K). Double and single bars indicate 250 and 50 μm , respectively.

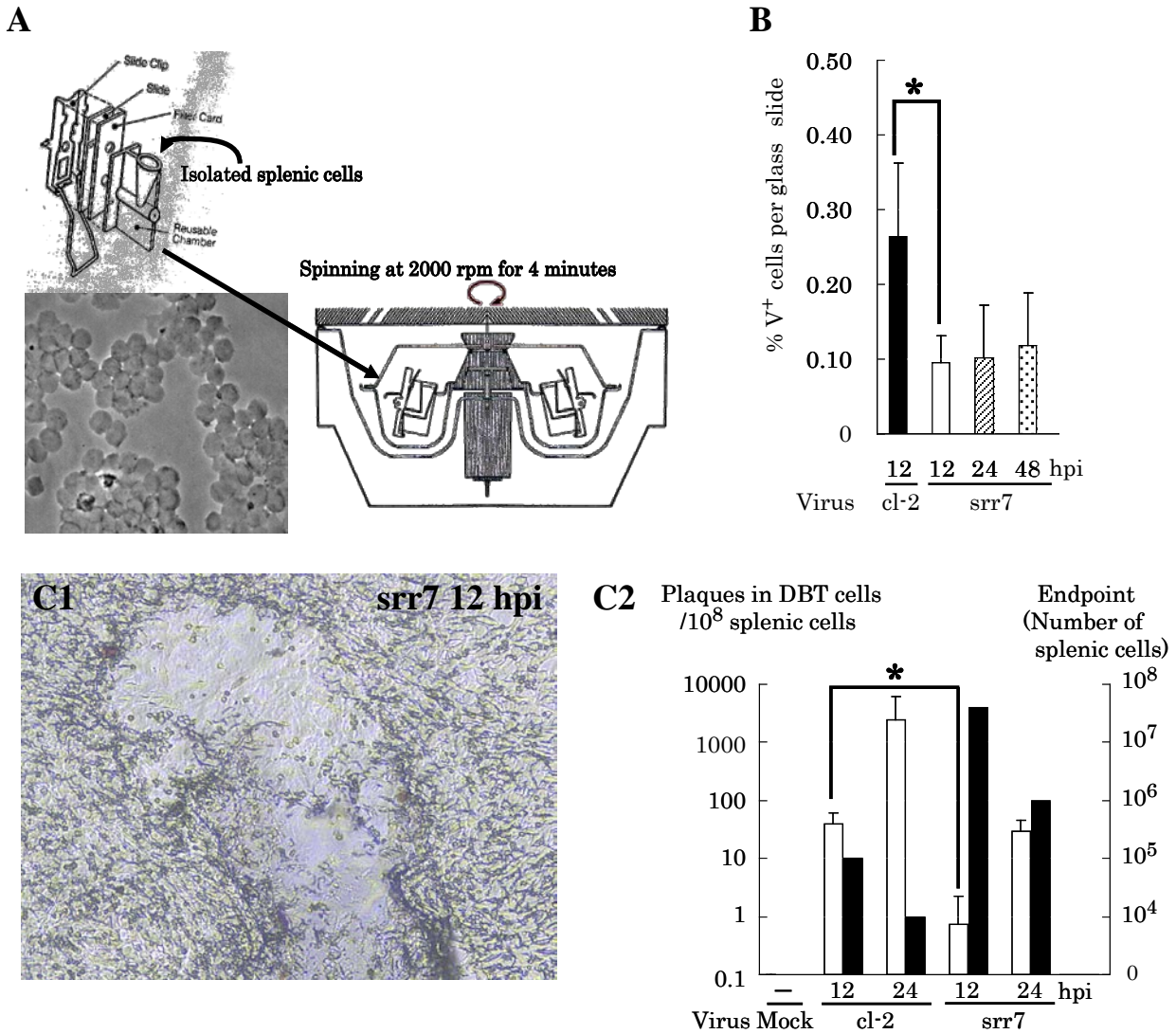


Figure 3 Cytopspin procedure

A: Schematic of cytopspin procedure. B: Infected cell population of splenic cells detected by immunofluorescence-based counting on glass slides after cytopspin. Viral antigen-positive cell numbers were counted while viewing whole areas mounted on glass slides, and the total number of splenic cells on each glass slide was estimated from the cell number counted in 20 randomly selected fields (see Materials and Methods). The percentages of infected cells were ascertained after averaging the cell populations obtained from 3 prepared glass slides. C1: Induction of fusion in DBT cells by overlaying splenic cells after *srr7* infection at 12 hours pi. C2: Ratios of splenic cells producing infectious viral particles were estimated by counting plaques produced after co-culture with DBT cells for 24 hours (white bars). Black bars indicate cell numbers at endpoints where viral particle-producing splenic cells were not detected.

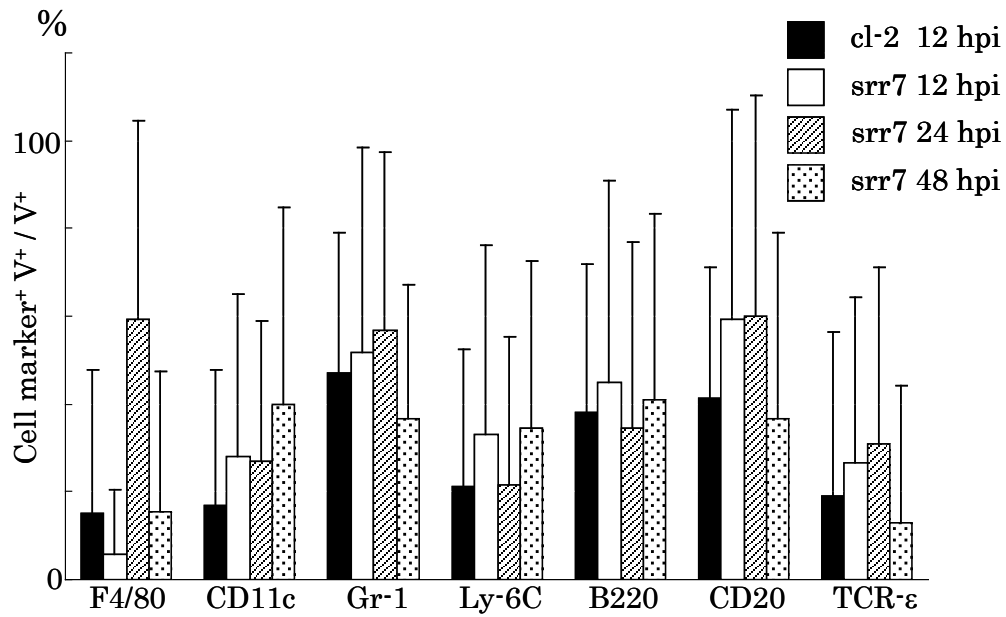


Figure 4 Populations of V⁺ and cell marker-positive cells among V⁺ cells

Populations were calculated after double immunofluorescent staining for each cell marker indicated in the figure and for viral antigens in the splenic cells collected and mounted on glass slides by cytopspin. Averaged percentages and SDs were obtained by counting fluorescence-positive cells in photographs taken from 20 randomly selected fields at x40 in each glass slide. The number of total cells per field ranged from 66 to 635 in 660 fields, whereas that of V⁺ cells ranged from 1 to 9 per field in 560 fields.

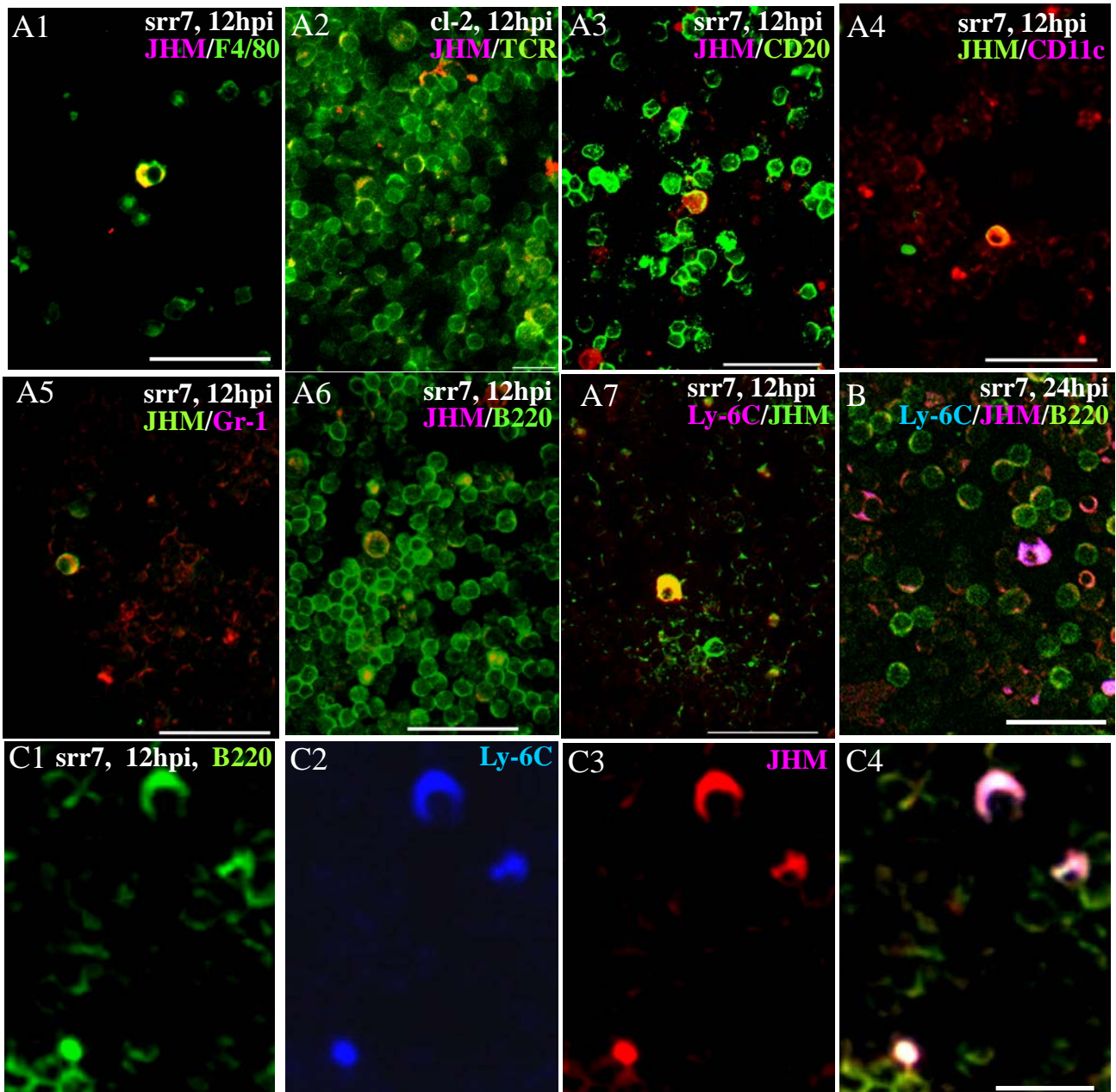


Figure 5 Immunofluorescence staining of Cytospin slides

A-C: Immunofluorescence with double (A) and triple staining (B, C) for F4/80, CD11c, CD20, TCR, Gr-1, B220, Ly-6C or viral antigens (indicated as JHM) in splenic cells after cytopsin prepared from mice infected with srr7 or cl-2 at 12 to 48 hours pi, as indicated in the pictures. Double-stained cells are observed as yellow cells or white cells. White bars indicate 25 μ m, respectively.

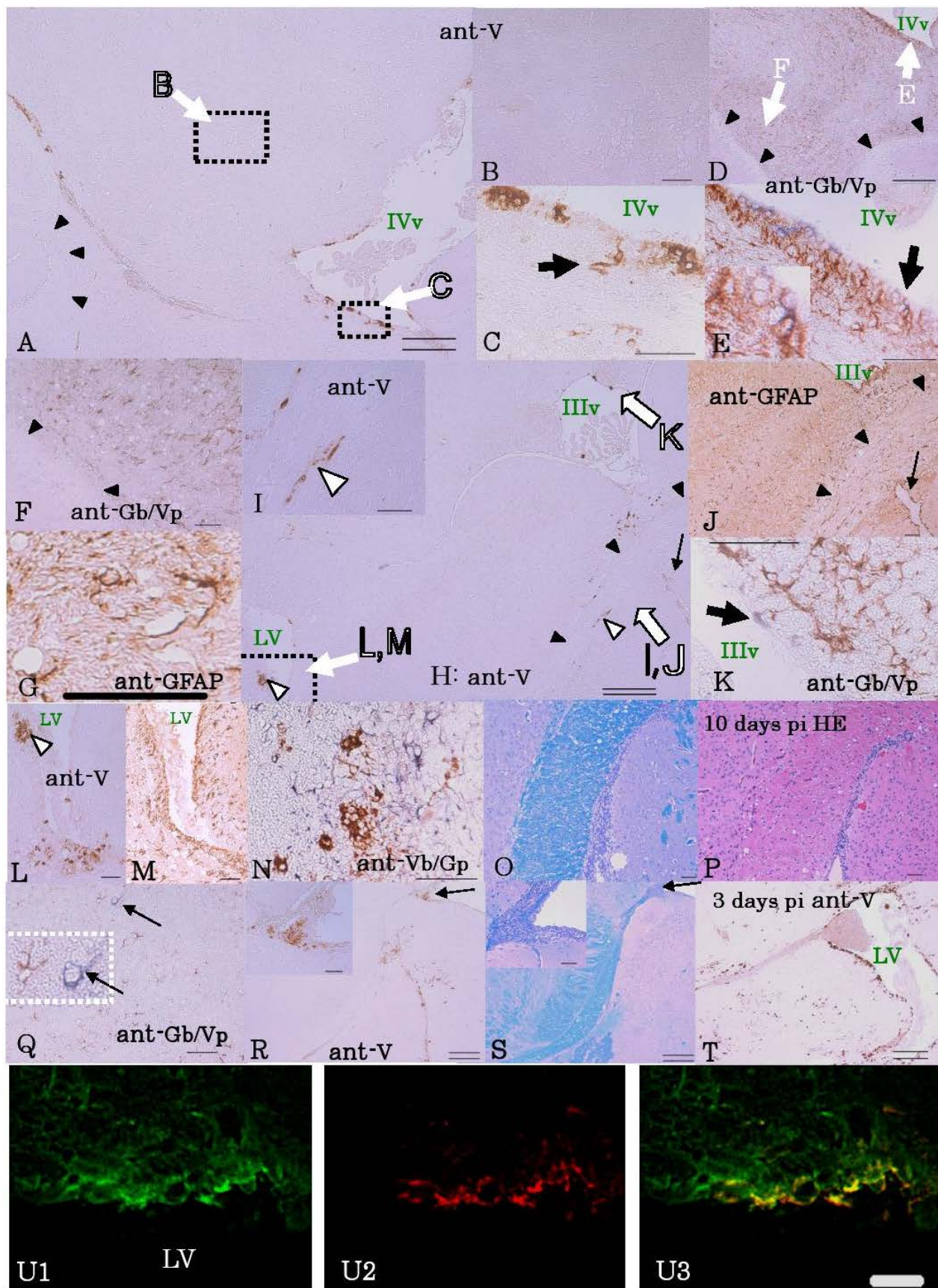
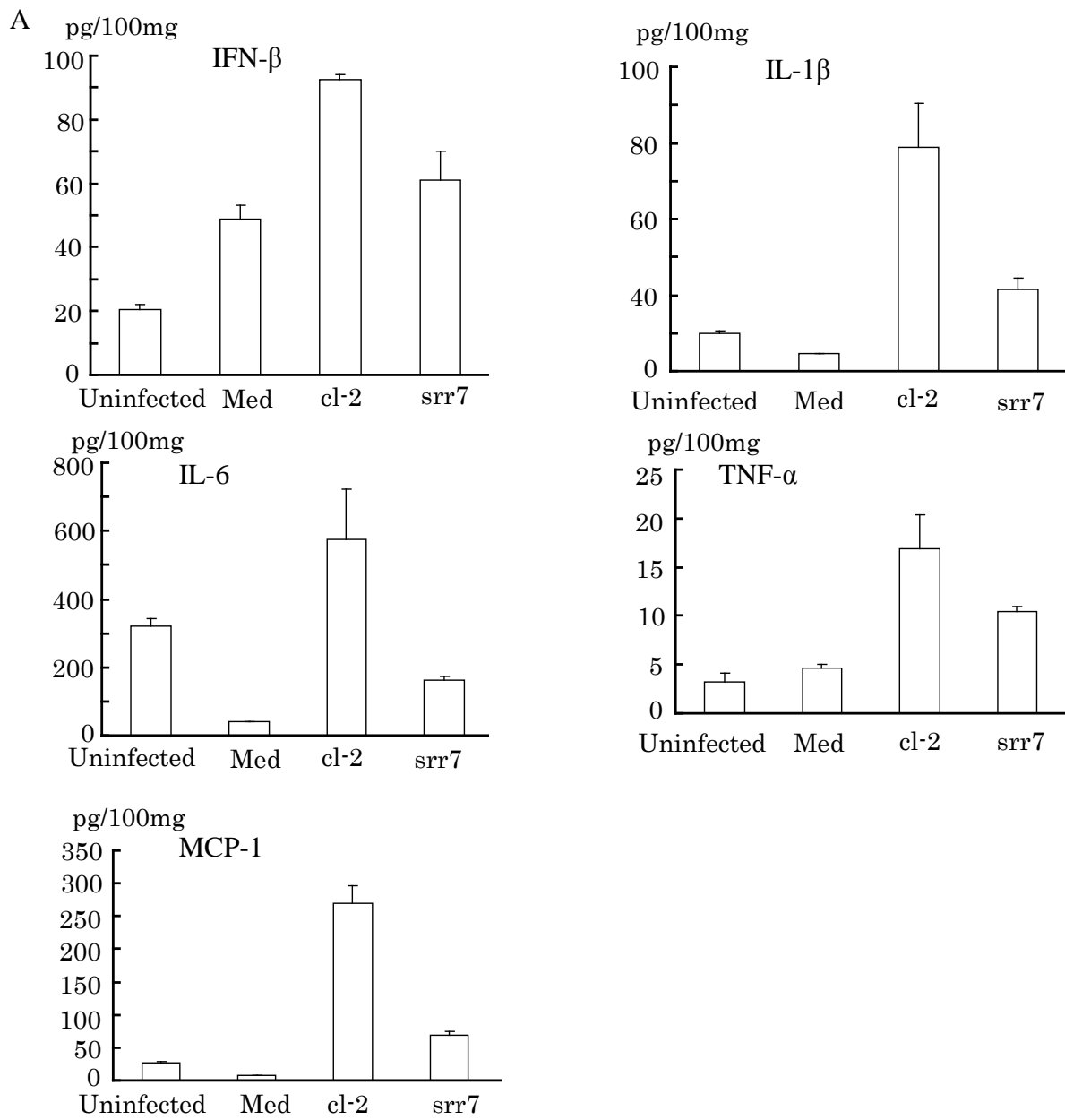


Figure 6 Vacuolar degeneration during the early phase of infection

All of the pictures were taken using paraffin-embedded materials, prepared from *srr7(H2)*-infected mice at 48 hours pi, except for P (10 days pi) and T (3 days pi). Immuno-histochemical staining was performed on serial sections to detect GFAP and the viral antigens, illustrated in the pictures as ant-GFAP (G, J, and M) and ant-V (A, B, C, H, I, L, R, and T), respectively. For double staining, brown- or purple-colored products were obtained using DAB or 4-chloro-naphthol, respectively. Brown-colored GFAP and purple-colored viral antigens are illustrated as ant-Gb/Vp (D, E, F, K, and Q), and brown-colored viral antigens and purple-colored GFAP as ant-Vb/Gp (N). (A) The pons and cerebellum around the fourth ventricle (IVv). Viral antigens are detectable only in the restricted area, namely around the IVv. Viral antigens are also visible in the area of the choroid plexus linked to the arachnoid (upper left in the picture). The area marked with arrowheads is the cerebellar granular layer. (B) A higher magnification of the dotted area with a white arrow and the letter B in (A). No viral antigens are detectable in spite of the vacuolar degeneration in this area. (C) A higher magnification of the dotted area with a white arrow and the letter C in (A). Most of the viral antigens are located in the surface area facing the fourth ventricle. Note that the antigen-positive cell indicated by the bold arrow has a narrow cytoplasm reaching the surface. (D) Double staining for GFAP (brown) and viral antigens (purple) in the area of the cerebellar white matter on a serial section next to the one stained for A-C. The upper left side is the fourth ventricle, and the areas marked by arrowheads are the granular layer. (E) A higher magnification of the area indicated by the letter E in (D). In the upper part is a line of cells that is purple-colored singly. The cell indicated by the bold arrow is double-stained, and shown at a higher magnification in the left bottom corner. (F) A higher magnification of the area indicated by the letter F in (D). Many GFAP-positive cells are present and vacuolar degeneration has spread, but no viral antigens are detectable. (G) In the same area as shown in (F), a higher magnification image shows a fine structure of the GFAP-positive cytoplasm attached to the vacuolation. (H) An area around the third ventricle (IIIv), lateral ventricle (LV), and corpus callosum indicated by black arrowheads. (I) A higher magnification of the area indicated by the letter I in (H). Here, the viral antigens are expressed along the fiber tract. (J) A serial section next to the one stained in (H). The thin black arrow indicates the same blood vessel shown in (H). In the corpus callosum indicated by black arrowheads, the astroglial reaction is not as prominent as in the other areas. (K) The area indicated by the letter K in (H). Here, the viral antigens (purple) are expressed solely on the ependymal cell. (L and M) A higher magnification of the area indicated by the letter L, M in (H). Here, the viral antigens are closely associated with the vacuoles. (N) The viral antigens (brown) and GFAP (purple) expression in the SVZ around the frontal portion of the LV. (O) A serial section next to the one stained in (N) was stained with HE & LFB to show that only a few vacuoles are formed around this area in spite of the appearance of many viral antigens and gliosis. (P) The same area as shown in N and P at 10 days pi, where no exSpongi developed. The vacuolar degeneration observed in this image was scored as grade 1 spongiosis (see Materials and Method). (Q) A solitary viral antigen-positive cell occasionally found at 48 hours pi in the thalamus (arrow) is shown at a higher magnification in the dotted area. Note that the glial reaction is not prominent here. (R) Distribution of viral antigens in the junctional area between the meninx (upper right side), choroid plexus, and ventricle. Many inflammatory cells in the meninx bear viral antigens (arrow and shown at a higher magnification in the upper left corner). (S) HE & LFB staining of the serial section next to the one stained in (R). (T) At 3 days pi, viral antigen expression becomes prominent in the brain parenchyma. (U) Some of the nestin-positive cells (green) in the SVZ are positive for viral antigens (red). LV indicates the lateral ventricle. Double and single bars indicate 250 and 50 μm , respectively. Single bar in U indicates 25 μm .



B

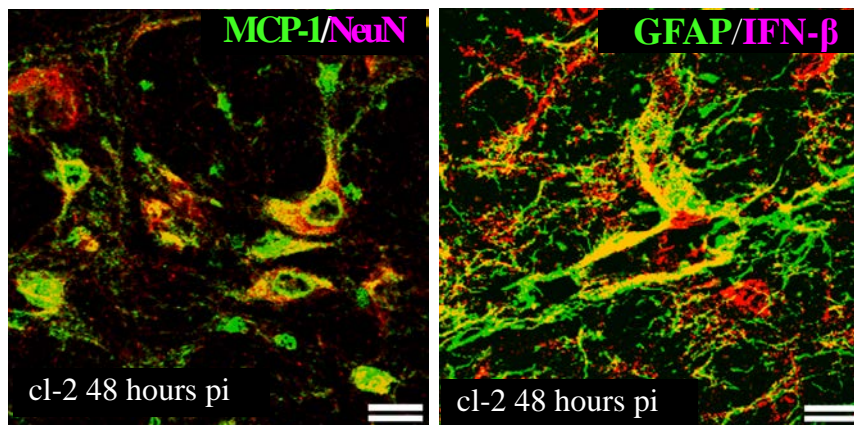


Figure 7 Cytokine production in the brain

A: The amount of cytokines in the pons obtained from mice inoculated with cl-2, srr7 or sham-inoculated with medium (Med) at 48 hpi, or untreated mice is measured by multiplex bead-based immunoassay; pg per 100 mg of tissue was shown. Vertical lines indicate SD. * and ** indicate the p-value (p) calculated by Student's t-test at <0.05 and <0.005 levels of significance, respectively. B: Immunofluorescence revealed cytokines was expressed in neurons and astrocytes.

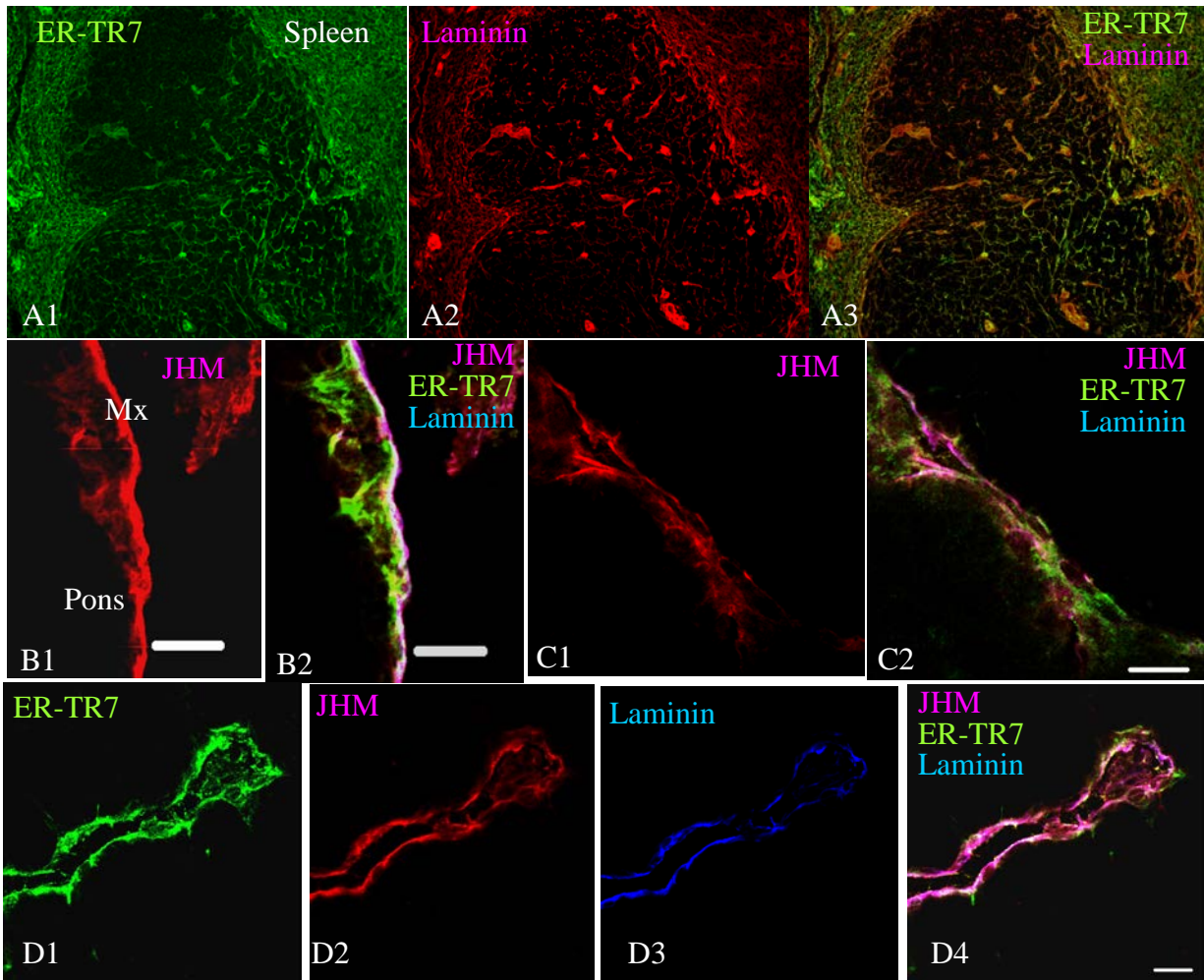


Figure 8 Triple immunofluorescence studies of ER-TR7 (green), viral antigen (red) and laminin (blue)

(A) Spleen was stained with anti-ER-TR7 and laminin antibody using in this study. (B, C) Viral antigens were colocalized with ER-TR7 and Laminin in the brain. Note the fibrous structures positive for viral antigens. (D) An architecture of blood vessels in the pons positive for ER-TR7 (green), viral antigens (red), and laminin (blue). 20 μ m.

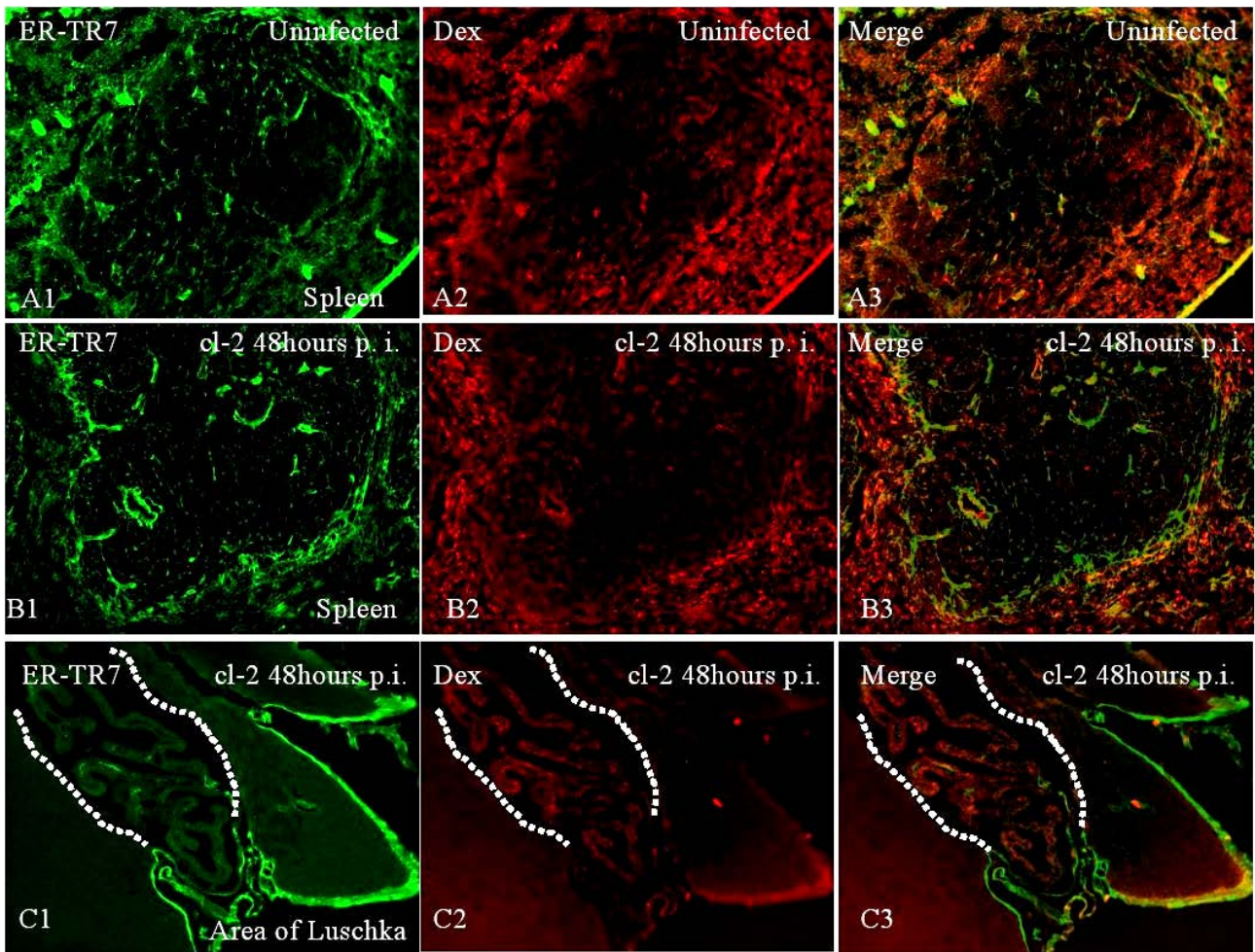


Figure 9 In vivo administration of fluorescent dextrans and their localization in the spleen (A, B) and brain (C)

(A, B) Localization of fluorescent-labeled dextran (Dex) within the spleen. (C) Fluorescent-labeled dextran in the foramen of Luschka of infected mice. Strong fluorescence signals were detected in the foramen of Luschka on 48 hours after infection with cl-2.

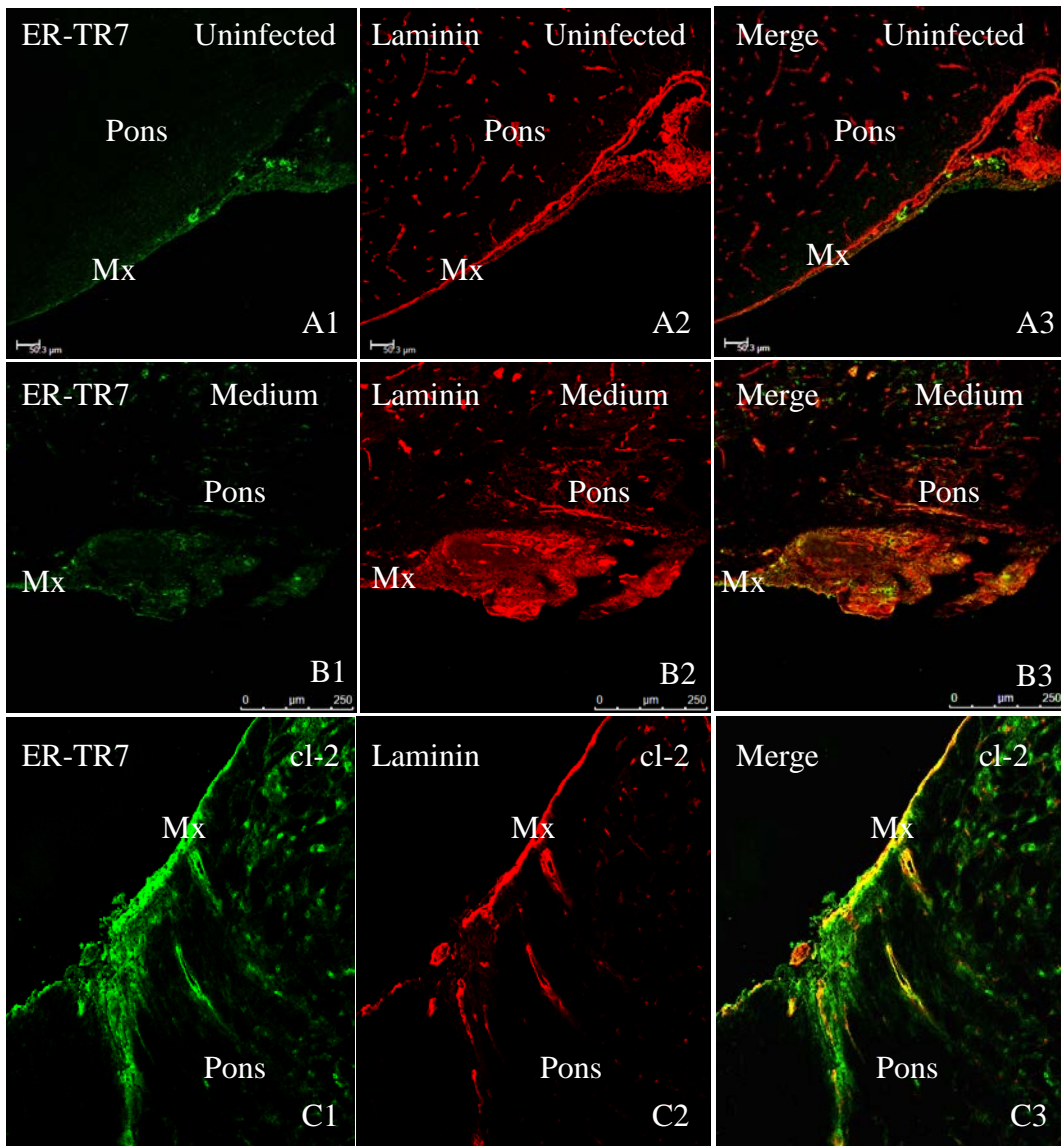


Figure 10 ER-TR7 expression in the brain

Immunohistochemical analysis of ER-TR7 in infected brain in association with laminin; in normal and infected brains are shown.

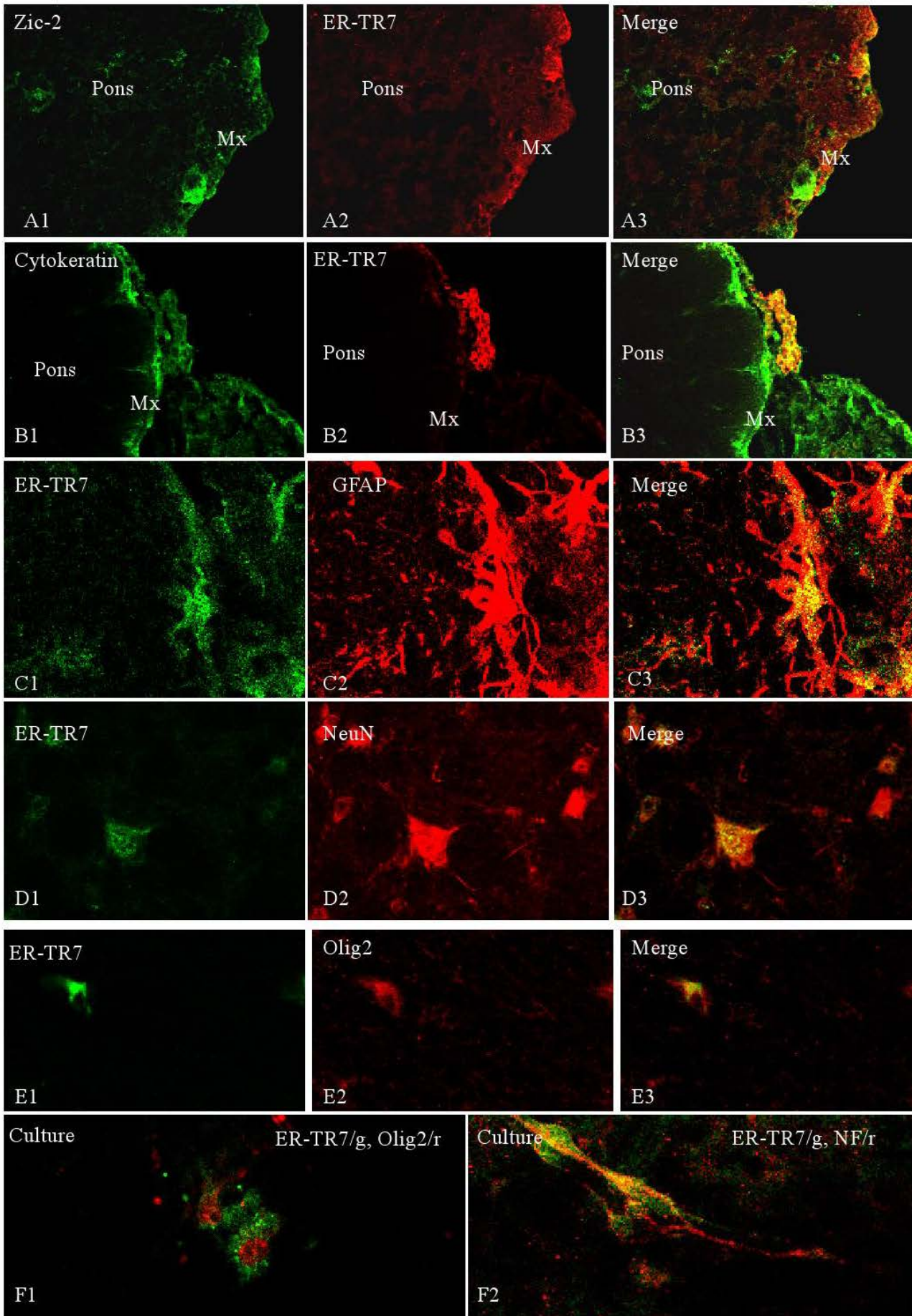


Figure 11 ERag-positive cells in the brain and primary culture

(A-E) Characterization of parenchymal cells in the pons with arachnoid cell marker or neuronal and glial proteins by immunofluorescence. (F) Characterization of the cultured cells with neuronal and glial proteins by immunofluorescence. Primary cell cultures from mice were also stained by immunofluorescence with anti-ER-TR7 antibodies and antibodies to neural cell markers. Cells from 24 hours were fixed in ethanol and acetone. Immunofluorescent analysis was performed using anti-ER-TR7 (green), anti-NF (red), and anti-Olig2 (red) antibody to stain neuron-specific protein and glial protein as described in the text.

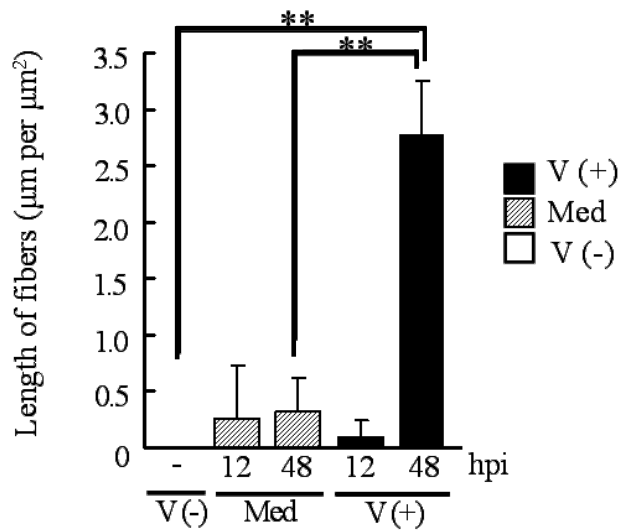
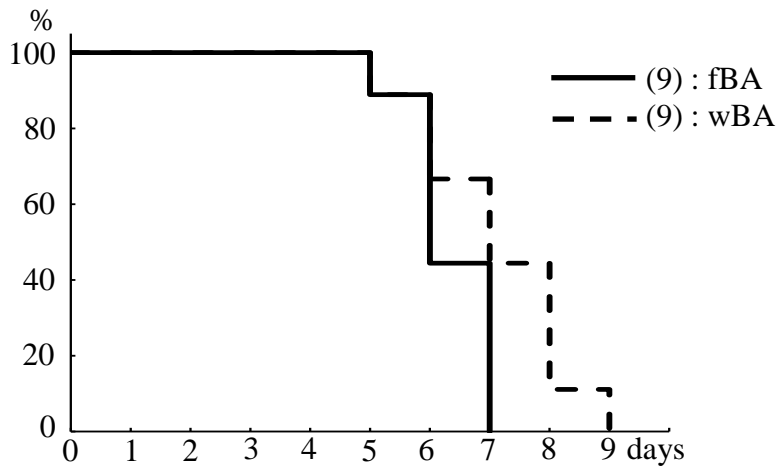


Figure 12 ER-TR7-antigen⁺ fibers in the fourth ventricle

The average length per μm^2 of ER-TR7-positive fibers associated with laminin expression in IVv obtained from three independently treated mice for each group. Vertical lines indicate SD. * and ** indicate the p-value (p) calculated by Student's t-test at <0.05 and <0.005 levels of significance, respectively.

A Viral Titers



B Viral Titers

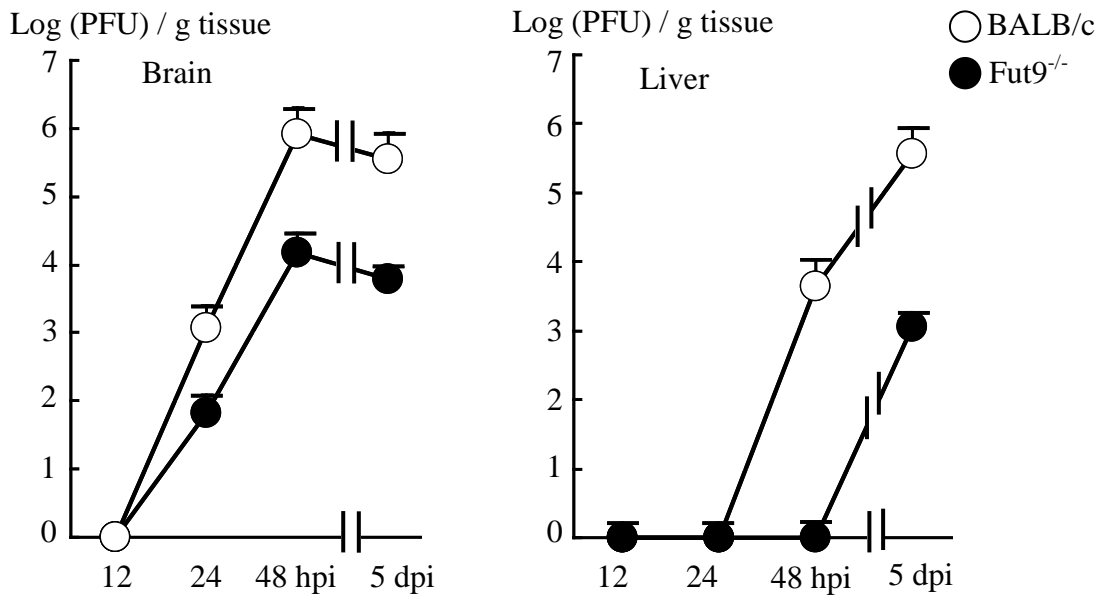


Figure 13 Virulence of the viruses

(A and B) srr7 viruses were used to inoculate the brains of wild-type BALB/c (open circles), or Fut9^{-/-} mice with a genetic background of BALB/c (closed circles). (A) Survival after infection. Numbers in parenthesis indicate the number of mice examined. (B) Viral titers measured as plaque forming units (PFU) per one gram of the brain or liver.

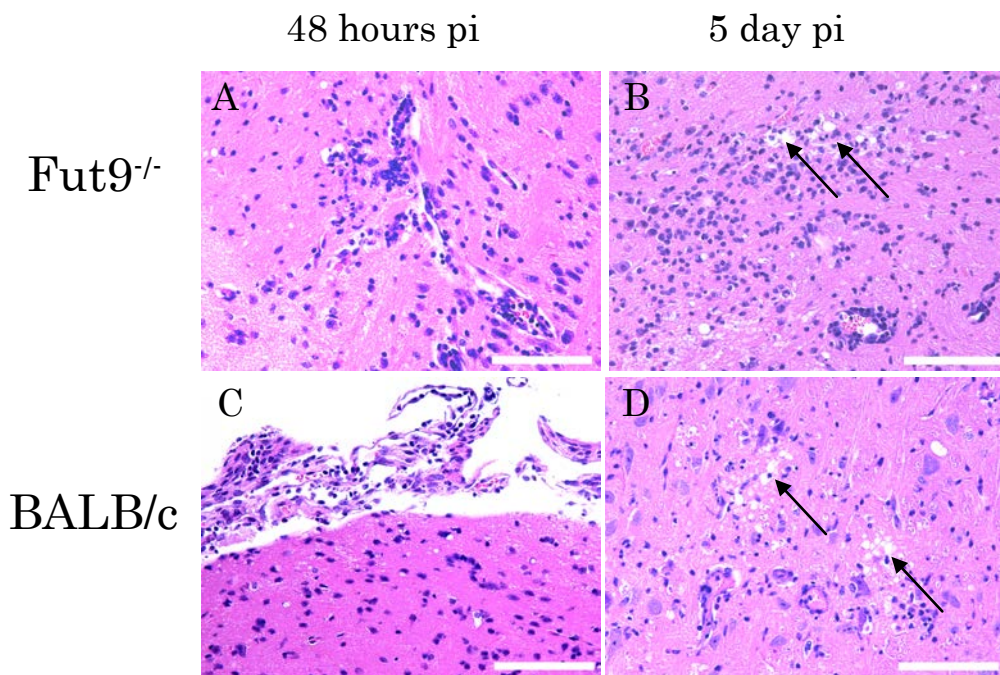
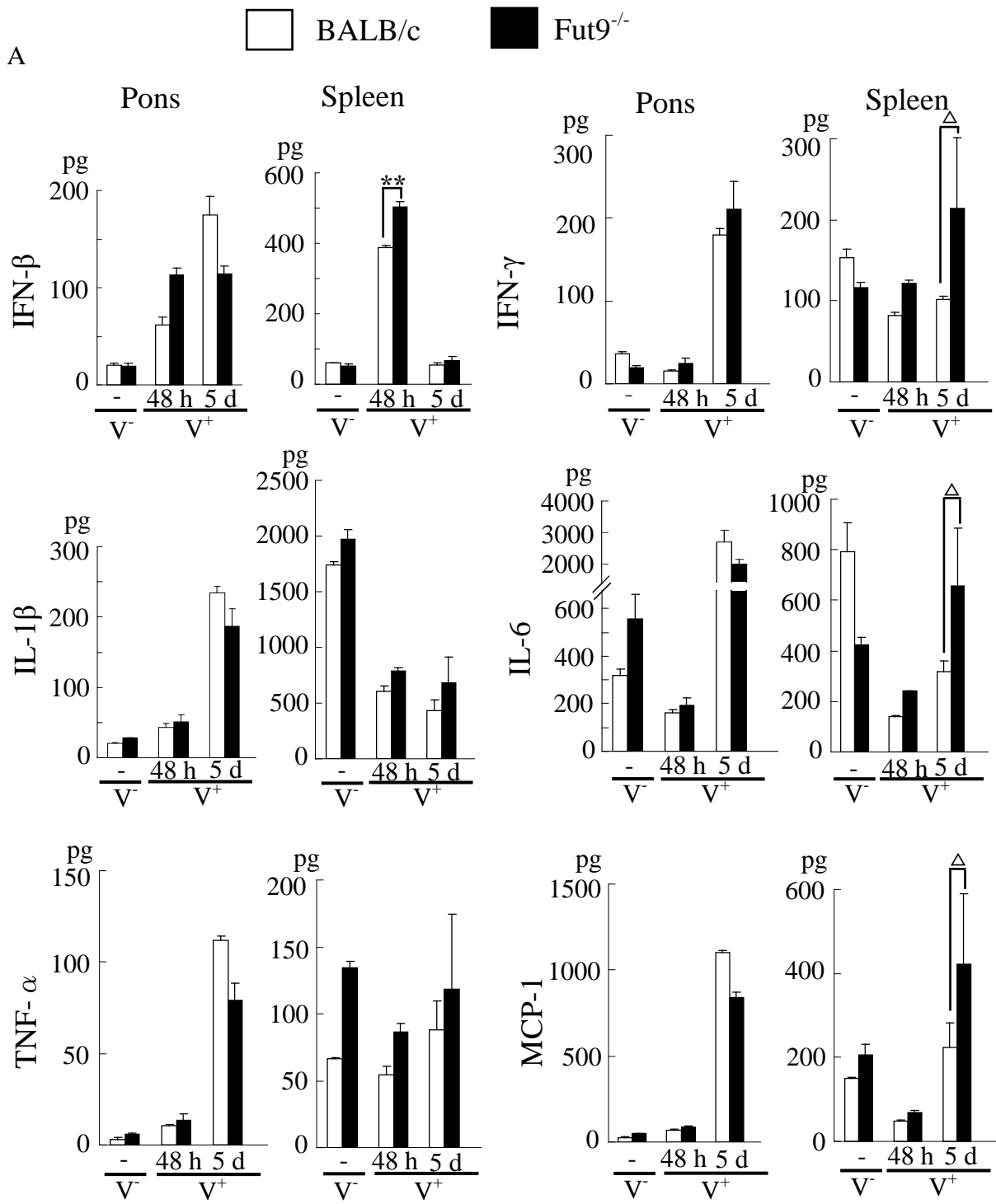


Figure 14 Histopathology in the brain and spleen

Wild-type and *Fut9*^{-/-} mice inoculated with *srr7* were sacrificed at 48 hours (A, C) and 5 days (B, D) post-inoculation (pi). Paraffin-embedded sections obtained from the brain were stained with HE. Arrows in B and D indicate the areas of spongiotic degeneration, which is a typical pathology in *srr7* infection. Bar indicates 100 μ m.



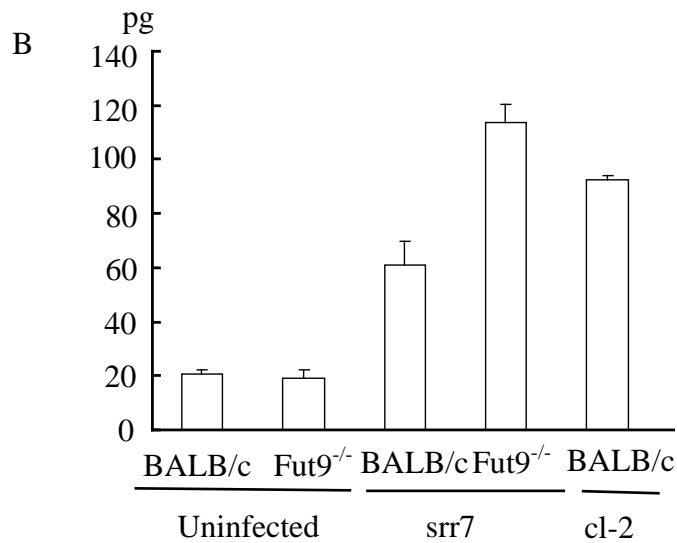


Figure15 Cytokine production

(A) At 48 hours and 5 days after *srr7* infection, tissue samples were collected and levels of cytokines were measured by luminex bead multiplex cytokine assays. (B) IFN- β production in the pons obtained from uninfected and *srr7*-infected wild-type and *Fut9*^{-/-} mice compared with that in *cl-2*-infected wild-type mice at 48 hours after infection. Results are displayed as the average with the standard deviation (SD) of duplicate wells. Cytokine levels were expressed in pg/100mg tissue (pons) or pg/spleen.

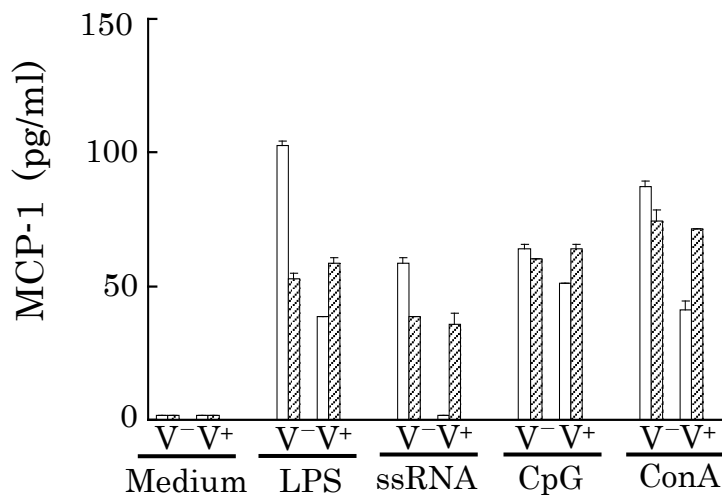


Figure 16 Cytokine production after stimulation

Splenocytes from mice infected with *srr7* for 48 h were stimulated with Toll-like receptor (TLR) ligands or ConA in vitro. Spleen cells (2×10^6 cells/ml) from BALB/c (open bars) or *Fut9*^{-/-} (hatched bars) mice were stimulated for 24 hours with several stimuli as indicated. Production of MCP-1 was quantified by luminex bead multiplex cytokine assays. Data are expressed as average \pm SD. Open and hatched bars represent levels of cytokines in wild-type and *Fut9*^{-/-} mice, respectively.

Antibody	Host	Dilution	Source
SP-1	Rabbit	1:200 (IHC, IF)	—
E2	Mouse	1:2 (IF)	—
F4/80	Rat	1:100 (IHC, IF)	Serotec or eBioscience
CD11b	Rat	1:50 (IF)	BD Biosciences
GFAP	Rabbit	1:100 (IHC)	Russel
GFAP	Mouse	1:250 (IHC, IF)	Sigma
CD3ε	Hamster	1:5 (IF)	Biolegend
B220	Rat	1:2.5 (IF)	BD Pharmingen
CD11c	Hamster	1:20 (IF)	ANA SPEC
Ly-6C	Rat	1:500 (IF)	BMA Biomedicals
CD20	Goat	1:50 (IF)	Santacruz Biochemistry, Inc.
ER-TR7	Rat	1:10 (IF)	Serotec
ER-TR7	Rat	1:10 (IHC)	BMA Biomedicals
Laminin	Rabbit	1:200 (IF)	LSL
NeuN	Mouse	1:10 (IF)	Chemicon
Olig2	Rabbit	1:100 (IF)	Millipore
Zic2	Rabbit	5μg/ml (IF)	Millipore
Cytokeratin	Mouse	5μg/ml (IF)	Sigma
NF	Goat	1:20	

Table 1 Antibodies used in this study

IF, immunofluorescent staining; IHC, immunohistochemistry

GFAP, glial fibrillary acidic protein

NeuN, neuronal nuclei

Olig2, oligodendrocyte lineage transcription factor 2

Zic2, zinc-finger transcription factor 2

NF; Neurofilament